# MLLM4TS: Leveraging Vision and Multimodal Language Models for General Time-Series Analysis

**Anonymous authors**Paper under double-blind review

000

001

002

004

006

008 009 010

011

013

014

015

016

017

018

019

020

021

022

024

025

026

027

028

029

031

032

034

037

038

040

041

042 043

044

046

047

048

051

052

# **ABSTRACT**

Effective analysis of time series data presents significant challenges due to the complex temporal dependencies and cross-channel interactions in multivariate data. Inspired by the way human analysts visually inspect time series to uncover hidden patterns, we ask: can incorporating visual representations enhance automated time-series analysis? Recent advances in multimodal large language models have demonstrated impressive generalization and visual understanding capability, yet their application to time series remains constrained by the modality gap between continuous numerical data and discrete natural language. To bridge this gap, we introduce MLLM4TS, a novel framework that leverages multimodal large language models for general time-series analysis by integrating a dedicated vision branch. Each time-series channel is rendered as a horizontally stacked color-coded line plot in one composite image to capture spatial dependencies across channels, and a temporal-aware visual patch alignment strategy then aligns visual patches with their corresponding time segments. MLLM4TS fuses fine-grained temporal details from the numerical data with global contextual information derived from the visual representation, providing a unified foundation for multimodal timeseries analysis. Extensive experiments on standard benchmarks demonstrate the effectiveness of MLLM4TS across both predictive tasks (e.g., classification) and generative tasks (e.g., anomaly detection and forecasting). These results underscore the potential of integrating visual modalities with pretrained language models to achieve robust and generalizable time-series analysis.

### 1 Introduction

Time-series analysis is a critical task across diverse fields, including manufacturing, finance, health-care, and environmental monitoring (Hamilton, 2020). It involves monitoring processes (Xu et al., 2022), predicting outcomes (Lim & Zohren, 2021), detecting anomalies (Liu et al., 2024c), and supporting data-driven decision-making (Mahalakshmi et al., 2016). Despite its broad utility, effective analysis remains challenging due to the complex dependencies of sequential data, the integration of multichannel and multimodal signals, and the diversity of tasks requiring application-specific methods. These challenges underscore the need for a unified, generalizable framework that can address a wide range of time-series analysis tasks efficiently and effectively.

Motivated by the observation that analysts often visualize time series to aid interpretation, we consider the role of visual perception in supporting analytical tasks. In anomaly detection as depicted in Figure 1, for instance, anomalies often manifest as visually salient regions - features that visually stand out to enable our eye-brain connection to quickly focus on the most important regions. Similarly, in classification tasks, characteristic motifs or recurring patterns are often preserved in the shape of the time series, serving as indicators of the corresponding class label, much like when a physician examines a patient's electrocardiogram (EKG) for diagnostic purposes. These insights lead to a natural question: *can we mimic human-like visual perception by integrating visual representations into time-series analysis to enhance model performance?* 

The emergence of foundation models has initiated a paradigm shift, offering a new lens through which to approach diverse downstream tasks (Bommasani et al., 2022). These models demonstrate remarkably few-shot generalization capabilities, often outperforming task-specific architectures. In

particular, large language models (LLMs) have shown potential for processing and reasoning over data with temporal dependencies (Gruver et al., 2023; Jin et al., 2024), opening up new avenues for advancing time-series analysis. Moreover, recent progress in large vision models has significantly enhanced visual understanding (Dosovitskiy et al., 2021; Liu et al., 2024b), motivating us to explore whether similar capabilities can be leveraged for time-series tasks through visual representation.

However, existing methods for adapting LLMs to time series data often have limitations. One fundamental challenge stems from a modality mismatch: while LLMs are pretrained on discrete token sequences, time series data are inherently continuous, leading to a notable discrepancy (Gruver et al., 2023; Ni et al., 2025). Moreover, many approaches adopt patching strategies that segment time series into smaller chunks (Nie et al., 2022; Wang et al., 2024). Yet, determining an appropriate patch size is non-trivial. If the patches are too large, critical temporal

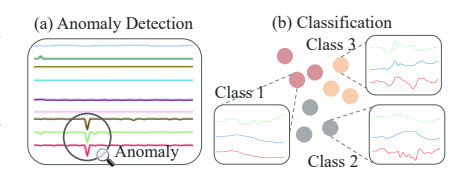


Figure 1: Illustration of the effect of time series visual inspection.

information within each segment may be lost. Conversely, if the patches are too small, the model might overemphasize local features and miss the global temporal patterns in the data. Furthermore, many current methods adopt a channel-independent (Nie et al., 2022; Zhou et al., 2023) approach when dealing with multivariate time series data, neglecting the cross-channel dependencies that recent studies have shown to be essential for capturing the complete dynamics of multivariate time series (Wu et al., 2020; Qiu et al., 2025).

In this paper, we introduce the Multimodal Large Language Model for Time Series (MLLM4TS), a framework that leverages a multimodal foundation model for time-series analysis by utilizing both time series and vision modalities. To address the limitations of language-only models, MLLM4TS introduces a vision branch that transforms multivariate time series into color-coded line-plot images, enabling the capture of global and cross-channel patterns. Visual embeddings derived from a pretrained encoder are then fused with time-series embeddings to jointly model fine-grained temporal dynamics and high-level contextual information. Our contributions are summarized as follows:

- Modality bridging. By introducing a vision encoder pretrained for alignment with languagebased embeddings (Radford et al., 2021), MLLM4TS effectively bridges the modality gap between continuous time series and discrete natural language, mitigates sensitivity to patch size selection, and enhances its ability to address complex time-series tasks.
- **Temporal-visual alignment.** We introduce a temporal-aware visual patch alignment strategy, which strengthens the alignment between imaged and numerical time series by leveraging the inherent structural properties of time series plots.
- Versatility and generalization. The proposed framework demonstrates promising performance
  across mainstream time series tasks, including classification, anomaly detection, and forecasting,
  and exhibits robust generalization under few-shot and zero-shot learning settings.

The remainder of this paper is organized as follows: Section 2 provides an overview of related work. Section 3 presents the proposed MLLM4TS framework, detailing its architecture and multimodal fusion approach. Section 4 presents experimental results along with extensive ablation studies to provide deeper insights into the framework's effectiveness. Finally, Section 5 concludes the paper with a summary of findings and directions for future work.

# 2 RELATED WORK

This section reviews prior work in time-series analysis, beginning with traditional methods and followed by recent advances in LLMs, pretrained models, and multimodal learning.

**Traditional Time Series Methods.** Traditional time-series methods, such as ARIMA (Box & Jenkins, 1970), Exponential Smoothing (Hyndman & Athanasopoulos, 2018), and Matrix Profile (Yeh et al., 2016), often struggle with multivariate or high-dimensional data due to their inherent linear assumptions. Deep learning techniques, including RNNs (LSTMs (Hochreiter & Schmidhuber, 1997), GRUs (Cho et al., 2014)), and especially Transformers (Vaswani et al., 2017), have significantly improved performance in complex time series tasks by effectively capturing long-range temporal dependencies, particularly in multivariate contexts (Lim et al., 2021; Wen et al., 2022).

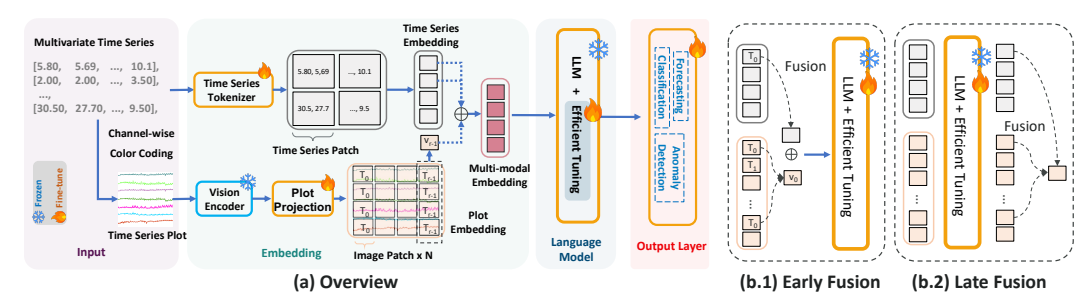


Figure 2: Overview of the MLLM4TS framework. (a) Multivariate time series are tokenized into patches and rendered as colour-coded line plots; the resulting embeddings are fused and passed to a pretrained LLM, followed by a task-specific output head. (b.1) Early fusion combines modalities before LLM processing. (b.2) Late fusion merges them after separate LLM encoding.

LLMs for Time Series. The success of LLMs in other domains (Hadi et al., 2023; Liang et al., 2024) has spurred interest in their application to time series. Directly adapting LLMs for time series remains challenging due to the inherent modality gap between continuous time series and discrete language data(Liu et al., 2024e; Tan et al., 2024). Techniques like prompt engineering and patch-based tokenization (Gruver et al., 2023; Nie et al., 2022; Zhou et al., 2023) attempt to bridge this gap, but challenges persist in capturing both global trends and local details, particularly in multivariate time series with complex cross-channel dependencies (Wu et al., 2020; Qiu et al., 2025).

**Pretrained Time Series Models.** Pretrained time-series models have shown promise, particularly in forecasting. Approaches such as Chronos (Ansari et al., 2024) and Moirai (Woo et al., 2024) leverage large-scale data to learn general representations but remain largely restricted to forecasting, with limited effectiveness on tasks like classification and anomaly detection. Similarly, MOMENT (Goswami et al., 2024) adopts a channel-independent design that hinders modeling of cross-channel dependencies. This task- and modality-specific orientation limits their applicability to broader time-series analysis, underscoring the need for more versatile models capable of addressing diverse tasks.

Multimodal Time-Series Analysis. Integrating multiple modalities, particularly visual representations, has shown promise in enhancing time-series analysis (Ni et al., 2025). Transforming time series into images, as in ViTST (Li et al., 2024), has proven effective for irregularly sampled time series classification tasks by leveraging pretrained vision transformers (Dosovitskiy et al., 2021). Furthermore, VisionTS (Chen et al., 2025) and Time-VLM (Zhong et al., 2025) utilize vision-language models for few-shot and zero-shot time series forecasting, while TAMA (Zhuang et al., 2024) employs GPT-40 for anomaly detection and interpretation. Nevertheless, these approaches remain specialized for individual downstream tasks, underscoring the need for more general multimodal architectures capable of robustly addressing diverse time-series applications.

Despite these advancements, a unified framework leveraging visual representations across a broad range of time series analysis tasks remains largely unexplored. This work addresses this gap by proposing MLLM4TS, a novel framework that integrates visual embeddings with LLMs to achieve robust and generalizable time series analysis across classification, anomaly detection, and forecasting.

# 3 MLLM4TS FRAMEWORK

The proposed MLLM4TS framework leverages pretrained vision and language models to capture complex temporal dependencies and enable multimodal fusion for time-series analysis. This section outlines the architecture and processing flow of MLLM4TS, as illustrated in Figure 2.

# 3.1 MODEL ARCHITECTURE AND COMPONENTS

The overall MLLM4TS framework comprises four key components: the input module, embedding module, language model, and output layer. We describe each component below.

(I) Input Module Given a multivariate time series  $\mathbf{x}_{1:L} = \{\mathbf{x}_1, \dots, \mathbf{x}_L\} \in \mathbb{R}^{L \times C}$  with L time steps and C channels, each channel is converted into a uniquely colored line plot to highlight cross-channel dependencies. These plots are horizontally stacked into a composite image (Figure 10) for the vision encoder, while the raw series is simultaneously input to the time-series tokenizer.

When the number of channels is large, plotting all of them leads to overlap and visual clutter. To address this, we adaptively adjust image size and apply dimensionality reduction by discarding highly correlated channels while preserving representative ones for visualization; the full time series is still maintained in the raw branch. Experiments in the following section show that this enhances plot clarity and that global structure derived from representative subsets remains beneficial.

(II) Embedding Module Each modality is encoded independently to produce embeddings in a shared feature space.

**Time Series Tokenizer.** The time series input is first normalized using reverse instance normalization (Kim et al., 2022), which normalizes the data based on its mean and variance, then added back to the processed output to enhance knowledge transfer. The normalized time series is then partitioned into non-overlapping patches (Nie et al., 2022), allowing the model to capture long-range temporal dependencies with fewer tokens. Finally, a linear projection layer maps each patch to the embedding dimension of the language model for subsequent processing.

Vision Encoder with Plot Projection. To model cross-channel dependencies and global patterns, each channel is transformed into a line plot, and the plots are aggregated into a composite image. A pretrained Vision-Language Model (VLM) (Zhang et al., 2024) processes this image to generate embeddings, with the visual encoder kept frozen for stability (Liu et al., 2024b;a). However, since most visual encoders are not pretrained to handle time series data, directly applying them without any adaptation may not achieve optimal performance in time-series applications. To address this, we introduce a plot projection module (a linear transformation) to adapt the visual embeddings for compatibility with the language model. This bridges the gap between channel-specific details and global information by leveraging visual data representations.

Multimodal Embedding Fusion. The embeddings generated by the time series tokenizer (time series embedding) and the plot projection (plot embedding) are combined, creating a unified representation of the input data. To better exploit the structural information embedded in time-series plots, we introduce a *Temporal-Aware Visual Patch Alignment* strategy, detailed in Section 3.2. This fusion enables the model to capture complementary information from both modalities, fine-grained temporal patterns and global cross-channel dependencies, thereby enhancing its understanding of complex temporal dynamics. In addition to the fusion strategy itself, we consider two fusion stages. In early fusion (Figure 2(b.1)), the time-series and visual embeddings are combined into multi-modal tokens prior to language model processing. In contrast, late fusion (Figure 2(b.2)) feeds both embeddings into the language model and combines them afterward.

(III) Language Model The core of MLLM4TS consists of a pretrained language model, adapted as a pivot to process embedded multimodal data and understand sequential data through a selective fine-tuning approach. Specifically, the self-attention blocks and Feedforward Neural Network (FNN) layers are kept frozen to retain the generalized knowledge acquired during pretraining. Meanwhile, the positional embeddings and layer normalization layers are fine-tuned, allowing the model to adapt more effectively to the characteristics of time series data. This efficient tuning strategy enables adaptation to new time series tasks with minimal task-specific data, leveraging both preserved pretraining knowledge and targeted fine-tuning (Lu et al., 2022).

(IV) Output Layer The output embeddings from the LLM are passed through a task-specific head to support a range of time series tasks, including classification, anomaly detection, and forecasting. For *classification*, a linear projection followed by a soft-max layer maps the embeddings to a probability distribution over the class set; the model is trained end-to-end with a cross-entropy loss. For *anomaly detection*, the head reconstructs the input sequence  $\hat{\mathbf{x}}_{1:L} = \{\hat{\mathbf{x}}_1, \dots, \hat{\mathbf{x}}_L\} \in \mathbb{R}^{L \times C}$ , and an anomaly score is computed from the discrepancy between the original series  $\mathbf{x}_{1:L}$  and its reconstruction. For *forecasting*, the head predicts the next F time steps  $\mathbf{x}_{L+1:L+F} = \{\mathbf{x}_{L+1}, \dots, \mathbf{x}_{L+F}\} \in \mathbb{R}^{F \times C}$ , where F denotes the forecast horizon. This modular design allows MLLM4TS to flexibly adapt the same backbone to diverse downstream tasks.

### 3.2 TEMPORAL-AWARE VISUAL PATCH ALIGNMENT

To process a two-dimensional line-plot image of a multivariate time series, let the image be  $\mathbf{I} \in \mathbb{R}^{H \times W \times C_I}$ , where (H, W) is the resolution of the image,  $C_I$  is the number of image color channels. The image is partitioned into non-overlapping square patches of size  $P \times P$  and processed by a

Vision Transformer (ViT) encoder (Radford et al., 2021). After flattening each patch, we obtain the sequence  $\mathbf{Z}_p \in \mathbb{R}^{N \times (P^2C_I)}$  with  $N = HW/P^2$  being the number of patches.

As the time series channels are stacked horizontally, the horizontal axis coincides with absolute time. The number of patches per row is r=W/P. Patches sharing the same horizontal index  $t\in\{0,\ldots,r-1\}$  correspond to the same time step; we group them as  $\mathcal{S}_t=\{\mathbf{Z}_p[t+kr]\mid k=0,\ldots,q-1\}$ , where q=H/P. Applying an aggregation function (e.g., average pooling) yields  $\mathbf{v}_t=\mathrm{Agg}(\mathcal{S}_t)\in\mathbb{R}^d$ , producing the sequence  $\{\mathbf{v}_t\}_{t=0}^{r-1}$  that is temporally aligned with the original signal as depicted in Figure 2. This alignment further removes the need for manual patch size tuning by setting the time-series patch size to L/r, where L is the time-series length. Finally, we adopt one-dimensional interpolation (upsampling or downsampling) to match the temporal resolution (i.e., length) of the time-series embedding, producing a temporally aligned multimodal representation.

#### 4 Experimental Analysis and Discussion

We conduct a comprehensive evaluation of MLLM4TS across mainstream time-series analysis tasks to address the following research questions (RQs). The key findings are presented in this section, while additional details are provided in the Appendix B.

- **RQ1.** Does incorporating visual representations enhance the performance of general time-series analysis tasks (Section 4.1)?
- *RQ2*. What types of visual representations (e.g., image layouts, visual encoders) are most effective when integrated into the MLLM4TS framework (Section 4.2)?
- RQ3. Are language models actually useful for multi-modal time-series analysis (Section 4.3)?

#### 4.1 PERFORMANCE OVERVIEW

**A Motivating Example.** Figure 3 presents a motivating example comparing input modalities for time-series classification on five randomly sampled UEA datasets (Bagnall et al., 2018).

The multi-modal approach consistently outperforms unimodal baselines, underscoring the importance of integrating local temporal and global contextual information for robust analysis.

Main Results. We evaluate MLLM4TS across three core time-series analysis tasks: classification (Section 4.1.1), anomaly detection (Section 4.1.2), and forecasting (Section 4.1.3), as well as zero-shot learning (Section 4.1.4). For each task, we outline the experimental setup and report results to evaluate the effectiveness of the proposed framework.



Figure 3: Performance comparison of using time series only, plot only, and the multimodal embeddings.

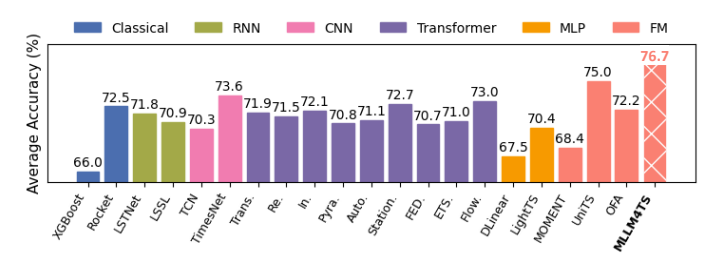
For fair comparison with the LLM-based TS-only framework OFA (Zhou et al., 2023), we adopt GPT-2 (Radford et al., 2019) as the language model backbone, consistent with prior sequential modeling work. For the vision encoder, we use CLIP-ViT-L-14 (Radford et al., 2021), pretrained for vision-language alignment and well-suited for visualized time-series data. Both MLLM4TS and the reproduced OFA baseline are evaluated over five random runs (error bars in Appendix B.1). Benchmark results are cited from original literature under the same protocol, or reproduced when unavailable. Full experimental details are provided in Appendix A.

#### 4.1.1 TIME-SERIES CLASSIFICATION

**Settings.** For the classification task, we follow the established benchmarking protocols (Zhou et al., 2023; Wu et al., 2023; Gao et al., 2024) on UEA datasets (Bagnall et al., 2018). These datasets, as shown in Table 5, include diverse time series data across domains such as sensor readings, EEG, audio, and speech. Each dataset provides different characteristics in terms of sequence length, number of classes, and data type, offering a comprehensive evaluation in diverse classification scenarios. The model is fine-tuned using cross-entropy loss to minimize classification error, and we apply cross-validation to ensure robust performance estimates.

**Results.** As shown in Figure 4, MLLM4TS outperforms these baselines, highlighting the advantages of its multimodal embedding and fine-tuning strategy.

The combination of time series tokenization and vision-based embeddings helps MLLM4TS capture both local temporal features and global cross-channel dependencies, resulting in improved classification accuracy across most datasets.



# 4.1.2 TIME-SERIES ANOMALY DETECTION

Figure 4: Model comparison in classification. "\*." in the Transformers indicates the name of \*former. The results are averaged from 10 subsets of UEA. See Table 8 for full results.

**Settings.** Anomaly detection in time series data is essential for

industrial applications, including health monitoring, space exploration, and environmental monitoring. However, progress in evaluating and benchmarking anomaly detection methods has been hindered by issues related to dataset quality, such as mislabeling, bias, and feasibility concerns (Wu & Keogh, 2021; Liu & Paparrizos, 2024). To ensure reliable comparison, we conduct our evaluation using the recently published TSB-AD-M benchmark (Liu & Paparrizos, 2024), a heterogeneous and curated collection comprising 200 multivariate time series (180 for evaluation) from six time series domains. A detailed description of datasets is provided in Table 6.

In addition, to address limitations of traditional evaluation measures - specifically their susceptibility to bias, lack of discrimination and adaptability (Liu & Paparrizos, 2024), we adopt the VUS-PR (Paparrizos et al., 2022; Boniol et al., 2025) as our evaluation measure. VUS-PR improves robustness by reducing sensitivity to temporal lag, enhances accuracy by minimizing bias across different scenarios, and promotes fairness by ensuring consistent evaluations under similar conditions. Additional evaluation results based on the imperfect yet widely employed point-adjusted F score are available in Table 10. For fair comparisons with baseline methods, we use mean squared error (MSE) as the reconstruction loss across all reconstruction-based approaches. During fine-tuning, MLLM4TS is trained to accurately reconstruct normal time series patterns, with anomalies expected to result in higher reconstruction errors.

Table 1: Model comparison in anomaly detection. The top five models from each category in the TSB-AD-M benchmark (Liu & Paparrizos, 2024) are presented, with the detailed evaluation provided in Table 9. VUS-PR is adopted as the primary evaluation measure. Higher values indicate better performance. The best performance is highlighted in bold, and the second-best is underlined.

Domain		S	Statistical					NN			FM		
	PCA (2017)	KMeansAD (2001)	CBLOF (2003)	MCD (1999)	OCSVM (1999)	CNN (2018)	OmniAnomaly (2019)	LSTMAD (2015)	USAD (2020)	AutoEncoder (2014)	OFA (2023)	MLLM4TS (Ours)	
Environment	1.000	0.862	1.000	1.000	0.810	0.998	0.813	0.991	0.813	0.997	0.909	1.000	
Facility	0.678	0.363	0.567	0.551	0.579	0.529	0.535	0.590	0.530	0.631	0.647	0.679	
Finance	0.103	0.020	0.032	0.060	0.024	0.022	0.021	0.022	0.021	0.028	0.156	0.143	
HumanActivity	0.278	0.093	0.137	0.163	0.113	0.165	0.197	0.183	0.197	0.142	0.110	0.122	
Medical	0.113	0.187	0.073	0.073	0.070	0.188	0.300	0.153	0.278	0.071	0.083	0.131	
Sensor	0.090	0.255	0.110	0.112	0.115	0.164	0.115	0.128	0.111	0.125	0.125	0.194	
TSB-AD-M	0.310	0.295	0.273	0.271	0.265	0.313	0.312	0.307	0.304	0.295	0.296	0.349	

**Results.** As shown in Table 1, MLLM4TS achieves a substantial improvement over its time-series-only counterpart, OFA, and attains the best overall performance in multivariate time series anomaly detection. It outperforms both statistical and neural network-based baselines, highlighting the effectiveness of introducing vision modality in identifying anomalies in time series.

# 4.1.3 TIME-SERIES FORECASTING

**Settings.** For multivariate time series forecasting, we follow the experimental protocol established by the recent LLM-based forecasting method AutoTimes (Liu et al., 2024e), which incorporates a diverse set of real-world datasets, including ETTh1 (Zhou et al., 2021), ECL, Traffic, Weather (Wu et al., 2021), and Solar-Energy (Liu et al., 2023). Detailed dataset descriptions are provided in the Appendix. To ensure a fair comparison, we adopt GPT-2 as the backbone for AutoTimes and fix the context length L=672 across all baselines. We adopt the "One-for-One" (Liu et al., 2024e)

evaluation across all methods (i.e., training a separate model for each forecasting horizon). Additional discussion on auto-regressive forecasting is provided in Table 16.

Table 2: Model comparison in forecasting. All the results are averaged from 4 different prediction lengths {96, 192, 336, 720}. The best performance is highlighted in bold, and the second-best is underlined. Full results are provided in Table 11.

Models	MLL:	M4TS irs)		FA (23)		onTS (25)		Times 24e)	Time (20	LLM (24)	Uni' (202	Гime 24d)	iTra (20		DLi (20	near (23)	Patcl (20		Time (20	esNet (23)
Metric	MSE	MAE	MSE	MAE	MSE	MAE	MSE	MAE	MSE	MAE	MSE	MAE	MSE	MAE	MSE	MAE	MSE	MAE	MSE	MAE
Weather	0.225	0.266	0.231	0.269	0.236	0.269	0.242	0.278	0.227	0.266	0.260	0.283	0.238	0.272	0.240	0.300	0.226	0.264	0.259	0.287
Solar.	0.188	0.246	0.229	0.296	0.231	0.266	0.197	0.242	0.234	0.293	0.254	0.291	0.202	0.269	0.217	0.278	0.189	0.257	0.200	0.268
ETTh1	0.408	0.430	0.426	0.438	0.398	0.415	0.397	0.425	0.409	0.432	0.438	0.445	0.438	0.450	0.423	0.437	0.413	0.431	0.458	0.450
ECL	0.165	0.261	0.167	0.264	0.157	0.251	0.173	0.266	0.170	0.275	0.194	0.287	0.161	0.256	0.177	0.274	0.159	0.253	0.192	0.295
Traffic	0.406	0.283	0.416	0.295	0.395	0.261	0.406	0.276	0.402	0.294	0.460	0.301	0.379	0.272	0.434	0.295	0.391	0.264	0.620	0.336

**Results.** As shown in Table 2, lower MSE and MAE values indicate better forecasting performance. Our multimodal approach achieves competitive results against established baselines, despite their meticulous design and optimization solely for forecasting task. This includes clear advantages on datasets exhibiting periodic patterns, such as Solar-Energy (a showcase provided in Figure 10). Furthermore, reducing the plotted channels to 50 in high-dimensional datasets like Electricity (321 channels) and Traffic (862 channels) consistently improves performance compared to visualizing all channels (details provided in Table 17). This reduction not only enhances clarity and scalability but also shows that global structural information extracted from representative subsets effectively preserves inter-channel interactions for forecasting.

#### 4.1.4 FEW/ZERO-SHOT LEARNING

**Settings.** LLMs have demonstrated strong few-shot and zero-shot learning capabilities in natural language tasks (Brown et al., 2020; Kojima et al., 2022). In this section, we investigate whether similar capabilities can be extended to time series analysis. For the few-shot setting, we use only 10% of the available training data to evaluate each model's ability to adapt to data-sparse environments.

For zero-shot learning, we assess the model's capacity for cross-domain generalization: specifically, we evaluate performance on a target dataset  $D_A$  without any direct training on it, assuming the model has been trained or pretrained on a different source dataset  $D_B$ . We compare MLLM4TS with both LLM-based baselines, including OFA (Zhou et al., 2023) and LLMTime (Gruver et al., 2023), as well as recent time series foundation models, such as



Figure 5: Performance comparison under (a) few-shot and (b) zero-shot settings. Results are reported using MSE (lower the better), averaged across four forecasting horizons {96, 192, 336, 720}. Full results are provided in Table 12 13.

Chronos (Ansari et al., 2024), Moirai (Woo et al., 2024), and MOMENT (Goswami et al., 2024).

**Results.** As illustrated in Figure 5, MLLM4TS outperforms its time-series-only counterpart under both few-shot and zero-shot learning conditions. In the zero-shot scenario, it also exceeds the performance of time series foundation models that are pretrained exclusively on numerical data, thereby demonstrating superior cross-domain generalization. These findings highlight MLLM4TS's rapid adaptation to previously unseen datasets and resilience to distribution shifts.

# 4.2 VISUAL REPRESENTATION ANALYSIS

With the promising results achieved by our multimodal strategy across mainstream time series analysis tasks, we further investigate the role of different visual representations. This analysis is conducted from four perspectives, as illustrated in Table 3: image layout, visual encoder choice, fusion stage, and sensitivity to patch size selection. For image layout, we compare two configurations: the horizontal layout, where each time series channel is stacked horizontally, and the grid layout, where each channel is plotted within a smaller subregion of the image (a visual example provided in Figure 9). Overall, the horizontal layout consistently outperforms the grid layout, highlighting the effectiveness of our proposed temporal-aware visual patch alignment for aligning visual and

time series modalities. To assess the impact of the visual encoder, we compare two representative architectures: CLIP (Radford et al., 2021), which is pretrained on vision-language alignment tasks, and ResNet (He et al., 2016), which is pretrained solely on image classification. CLIP consistently outperforms ResNet, underscoring its superior capability in processing visual representations of time series due to its alignment with language-based embeddings.

Moreover, we investigate the effectiveness of different fusion strategies, with particular focus on the stage at which modalities are integrated. Experimental results show that early fusion consistently achieves better performance, supporting the hypothesis that **low-level** correlations between imaged time series and numerical time series encode meaningful and complementary information for time-series analysis (Baltrušaitis et al., 2018; Mo

Table 3: Visual representation analysis on image layouts, visual encoders, fusion strategies, and patch-size sensitivity. Accuracy is reported for classification (CLF) and VUS-PR for anomaly detection (AD). Better performance is highlighted in bold. Full results are in Tables 14 and 15.

Task	Img Lay	out	Visu	alEnc	Fusion	nStage	PatchS	ize STD
	Horizontal	Grid	CLIP	ResNet	Early	Late	Plot-TS	TS-Only
CLF	76.7 0.349	75.2	76.7	72.6 0.348	76.7	73.5	0.56	1.13
AD	0.349	0.344	0.349	0.348	0.349	0.343	_	-

& Morgado, 2024). In addition to its predictive advantages, early fusion exhibits reduced computational cost, as it minimizes the number of tokens that need to be processed by the language model. A detailed runtime comparison is presented in Figure 6.

We further investigate the impact of the vision modality on the model's sensitivity to patch size selection. As shown in the "PatchSize STD" column of Table 3, we report the standard deviation of classification performance across different patch sizes (ranging from  $\{1,2,...,10\} \times L/r$ , see notation in Section 3.2). Note that for anomaly detection, patch size variation is not applicable, as each input instance corresponds to a fixed-length time series window. Compared to its TS-only counterpart, MLLM4TS exhibits lower performance variance, indicating greater robustness to patch size variation. This stability suggests that the temporal-aware visual alignment preserves the temporal structure more effectively and reduces the model's dependence on precise patch size selection.

#### 4.3 LANGUAGE BACKBONE ANALYSIS

With the growing debate over the effectiveness of LLMs for time-series analysis, recent studies have reported that LLM-based methods offer limited advantages over models trained from scratch and fail to adequately capture sequential dependencies in forecasting tasks (Tan et al., 2024). In this work, we extend the scope of investigation to include classification and anomaly detection, examining whether the language modeling capabilities of LLMs are beneficial across a broader range of time series tasks.

As shown in Table 4, we follow the LLM4TS ablation protocol introduced in (Tan et al., 2024), where "LLM" refers to a model using a GPT-2 backbone, and "LLM2Attn" replaces the language model with a single multi-head attention layer (i.e., PAttn, as proposed in the study). In the time-series-only setting, we observe similar trends reported in prior work: replacing the LLM with a simpler attention mechanism results in a 2.6% improvement in forecasting. However, for classification and anomaly detection, models utilizing the full LLM outperform the LLM2Attn variant.

In multimodal scenarios, the benefits of language modeling become more pronounced and consistent, where all three tasks, forecasting, classification, and anomaly detection, benefit from the use of LLMs. This highlights the effectiveness of combining a language-aligned vision encoder with LLMs and underscores the importance of language modeling capabilities for general-purpose multi-modal time series analysis.

Table 4: Comparison of performance between the LLM and LLM2Attn backbones. " $\Delta$  Perf" denotes the relative percentage by which LLM outperforms LLM2Attn (positive: LLM better; negative: LLM2Attn better). Results are averaged over 10 UEA datasets for classification (Accuracy), TSB-AD-M for anomaly detection(VUS-PR), and the Weather dataset for forecasting (MSE). See Appendix B.3 for details.

Task		TS-Only			Plot-TS (Our	:s)
	LLM	LLM2Attn	$\Delta$ Perf	LLM	LLM2Attn	$\Delta$ Perf
CLF	72.2	70.2	2.80%	76.7	71.4	6.90%
AD	0.296	0.286	3.40%	0.349	0.340	2.60%
Forecasting	0.231	0.225	-2.60%	0.225	0.252	12.00%

Despite the promise of language modeling for this task, scaling to billion-parameter models (Touvron et al., 2023; Yang et al., 2024) does not consistently yield improvements over smaller architectures such as GPT-2. This suggests that GPT-2-scale models are sufficiently expressive, while larger models

may introduce issues such as overfitting. Additional results on different language model backbones are provided in Appendix B.3.

We further investigate alternative tuning strategies and their associated runtime implications. As shown in Figure 6(a), the addition of the vision processing branch leads to notable performance gains, albeit at the cost of increased computational overhead. The late fusion strategy incurs a higher runtime due to the longer token sequences passed to the LLM. Furthermore, the TuneAll variants, which involve fine-tuning all model parameters, do not yield improved performance despite their significantly higher computational cost.

We also analyze the training time under different fine-tuning configurations as depicted in Figure 6(b). MLLM4TS adopts the tuning strategy described in Section 3.1, where the "Freeze" variant keeps the pretrained vision and language backbones fixed and updates only the task-specific linear head. In contrast, "TuneVis" further fine-tunes the vision encoder. Among these variants, MLLM4TS achieves the best overall performance while maintaining relatively low training cost, demonstrating the effectiveness of its selective fine-tuning strategy.

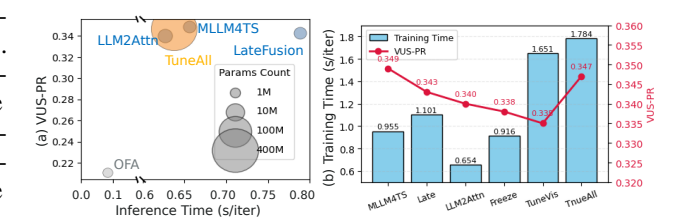


Figure 6: Efficiency evaluation of MLLM4TS and its variants on the TSB-AD benchmark (Liu & Paparrizos, 2024). (a) Inference time versus anomaly-detection performance (VUS-PR), with bubble area proportional to the number of tunable parameters. (b) Training runtime and corresponding VUS-PR, measured using a fixed batch size of 64.

## 4.4 DISCUSSION

432

433

434

435

436

437

438

439

440

441

442

443

444

445

446

447

448

449

450

451

452

453

454

455

456 457

458

459

460

461

462

463

464

465

466

467

468

469

470

471

472 473

474 475

476

477

478

479

480

481

482

483 484 485

We conclude this section by synthesizing research insights in response to the three research questions posed earlier. In this study, we employ a common and intuitive form of time series visualization - the time series line plot. Our findings indicate that incorporating visual representations can significantly enhance the performance of time series analysis by offering an additional modality of data representation, without requiring external information or domain-specific expert knowledge. Through systematic analysis of visual representations, we validate the benefits of exploiting structural patterns embedded in composite line plots and demonstrate the advantage of utilizing visual encoders pretrained on vision-language alignment. The superior performance of early fusion strategies highlights the presence of low-level correlations between imaged and numerical representations of time series data. Furthermore, our results underscore the importance of language modeling capabilities in multimodal time series analysis. The incorporation of a vision modality enhances performance but also introduces additional computational overhead. This observation motivates future work aimed at developing a lightweight visual encoder tailored to time series data, such as pretrained CLIP (Radford et al., 2021) for the time series domain. Overall, this work offers both a conceptual foundation and empirical evidence for the promise of multimodal large language models (Kong et al., 2025; Jiang et al., 2025), particularly in harnessing vision for advanced time series understanding (Ni et al., 2025).

### 5 CONCLUSION

In this paper, we introduced MLLM4TS, a unified multimodal framework for time-series analysis that leverages pretrained language models with vision-based encoders. By combining sequential and visual representations, MLLM4TS captures both local temporal patterns and global cross-channel dependencies, effectively addressing the complexities of multivariate time series. We evaluated its effectiveness on classification, anomaly detection, and forecasting across diverse datasets, demonstrating the complementary contributions of numerical and visual modalities. In summary, MLLM4TS offers a flexible solution for diverse time-series applications, opens avenues for incorporating additional aligned modalities such as images and videos, and motivates future work on lightweight encoders and more effective visual representations.

#### REPRODUCIBILITY STATEMENT

We have taken multiple steps to ensure the reproducibility of our work. A full description of the datasets, preprocessing procedures, and benchmark splits is provided in Appendix A.1. The architecture of MLLM4TS is detailed in Section 3, with additional implementation notes and pseudocode in Appendix A.2. Experimental protocols and evaluation metrics for classification, anomaly detection, forecasting, and zero-/few-shot learning are outlined in Section 4, with further results in Appendix B.

# REFERENCES

- Tao. https://www.pmel.noaa.gov/, 2006. URL https://www.pmel.noaa.gov/.
- Ahmed Abdulaal, Zhuanghua Liu, and Tomer Lancewicki. Practical approach to asynchronous multivariate time series anomaly detection and localization. In *Proceedings of the 27th ACM SIGKDD conference on knowledge discovery & data mining*, pp. 2485–2494, 2021.
- Charu C. Aggarwal. *Outlier Analysis*. Springer International Publishing, 2 edition, 2017. ISBN 978-3-319-47577-6. doi: 10.1007/978-3-319-47578-3. URL https://www.springer.com/gp/book/9783319475776.
- Abdul Fatir Ansari, Lorenzo Stella, Caner Turkmen, Xiyuan Zhang, Pedro Mercado, Huibin Shen, Oleksandr Shchur, Syama Sundar Rangapuram, Sebastian Pineda Arango, Shubham Kapoor, et al. Chronos: Learning the language of time series. *arXiv preprint arXiv:2403.07815*, 2024.
- Julien Audibert, Pietro Michiardi, Frédéric Guyard, Sébastien Marti, and Maria A Zuluaga. Usad: Unsupervised anomaly detection on multivariate time series. In *Proceedings of the 26th ACM SIGKDD international conference on knowledge discovery & data mining*, pp. 3395–3404, 2020.
- Marc Bachlin, Meir Plotnik, Daniel Roggen, Inbal Maidan, Jeffrey M Hausdorff, Nir Giladi, and Gerhard Troster. Wearable assistant for parkinson's disease patients with the freezing of gait symptom. *IEEE Transactions on Information Technology in Biomedicine*, 14(2):436–446, 2009.
- Anthony Bagnall, Hoang Anh Dau, Jason Lines, Michael Flynn, James Large, Aaron Bostrom, Paul Southam, and Eamonn Keogh. The uea multivariate time series classification archive, 2018, 2018.
- Tadas Baltrušaitis, Chaitanya Ahuja, and Louis-Philippe Morency. Multimodal machine learning: A survey and taxonomy. *IEEE transactions on pattern analysis and machine intelligence*, 41(2): 423–443, 2018.
- Rishi Bommasani et al. On the opportunities and risks of foundation models. *arXiv preprint* arXiv:2108.07258, 2022.
- Paul Boniol, Ashwin K Krishna, Marine Bruel, Qinghua Liu, Mingyi Huang, Themis Palpanas, Ruey S Tsay, Aaron Elmore, Michael J Franklin, and John Paparrizos. Vus: effective and efficient accuracy measures for time-series anomaly detection. *The VLDB Journal*, 34(3):32, 2025.
- George E. Box and Gwilym M. Jenkins. Time series analysis: forecasting and control. 1970.
- Tom B Brown et al. Language models are few-shot learners. In *Proceedings of the 34th International Conference on Neural Information Processing Systems*, pp. 1877–1901, 2020.
- Mouxiang Chen, Lefei Shen, Zhuo Li, Xiaoyun Joy Wang, Jianling Sun, and Chenghao Liu. Visionts: Visual masked autoencoders are free-lunch zero-shot time series forecasters. 2025.
- Tianqi Chen and Carlos Guestrin. Xgboost: A scalable tree boosting system. In *Proceedings of the 22nd ACM SIGKDD International Conference on Knowledge Discovery and Data Mining*, pp. 785–794, 2016.
- Kyunghyun Cho, Bart van Merrienboer, Dzmitry Bahdanau, and Yoshua Bengio. Learning phrase representations using rnn encoder-decoder for statistical machine translation. *arXiv preprint arXiv:1406.1078*, 2014.

- Angus Dempster et al. Rocket: Exceptionally fast and accurate time series classification using random convolutional kernels. *Data Mining and Knowledge Discovery*, 34:1454–1495, 2020.
  - Alexey Dosovitskiy et al. An image is worth 16x16 words: Transformers for image recognition at scale. In *International Conference on Learning Representations*, 2021.
    - Pavel Filonov, Andrey Lavrentyev, and Artem Vorontsov. Multivariate industrial time series with cyber-attack simulation: Fault detection using an lstm-based predictive data model. *arXiv* preprint *arXiv*:1612.06676, 2016.
    - Philippe Fleith. Controlled anomalies time series (cats) dataset, September 2023. Accessed: 2023-09-01.
    - Jean-Yves Franceschi et al. Unsupervised scalable representation learning for multivariate time series. In *Proceedings of the 33rd Conference on Neural Information Processing Systems*, pp. 4652–4663, 2019.
    - Shanghua Gao, Teddy Koker, Owen Queen, Tom Hartvigsen, Theodoros Tsiligkaridis, and Marinka Zitnik. Units: A unified multi-task time series model. *Advances in Neural Information Processing Systems*, 37:140589–140631, 2024.
    - Ary L Goldberger, Luis AN Amaral, Leon Glass, Jeffrey M Hausdorff, Plamen Ch Ivanov, Roger G Mark, Joseph E Mietus, George B Moody, Chung-Kang Peng, and H Eugene Stanley. Physiobank, physiotoolkit, and physionet: components of a new research resource for complex physiologic signals. *circulation*, 101(23):e215–e220, 2000.
    - Mononito Goswami, Konrad Szafer, Arjun Choudhry, Yifu Cai, Shuo Li, and Artur Dubrawski. Moment: A family of open time-series foundation models. In *International Conference on Machine Learning*, pp. 16115–16152. PMLR, 2024.
    - Scott David Greenwald. *Improved detection and classification of arrhythmias in noise-corrupted electrocardiograms using contextual information*. Thesis, Massachusetts Institute of Technology, 1990. URL https://dspace.mit.edu/handle/1721.1/29206. Accepted: 2005-10-07T20:45:22Z.
    - Nate Gruver, Marc Finzi, Shikai Qiu, and Andrew G Wilson. Large language models are zero-shot time series forecasters. *Advances in Neural Information Processing Systems*, 36:19622–19635, 2023.
    - Jiayi Gu et al. Lssl: A light-weighted model for scalable sequence learning on long time series. In *Proceedings of the International Conference on Learning Representations*, 2021.
    - Muhammad Usman Hadi, Rizwan Qureshi, Abbas Shah, Muhammad Irfan, Anas Zafar, Muhammad Bilal Shaikh, Naveed Akhtar, Jia Wu, Seyedali Mirjalili, et al. A survey on large language models: Applications, challenges, limitations, and practical usage. *Authorea Preprints*, 2023.
    - James D Hamilton. Time series analysis. Princeton university press, 2020.
    - Kaiming He, Xiangyu Zhang, Shaoqing Ren, and Jian Sun. Deep residual learning for image recognition. In *Proceedings of the IEEE conference on computer vision and pattern recognition*, pp. 770–778, 2016.
    - Zengyou He, Xiaofei Xu, and Shengchun Deng. Discovering cluster-based local outliers. *Pattern recognition letters*, 24(9-10):1641–1650, 2003.
  - Sepp Hochreiter and Jürgen Schmidhuber. Long short-term memory. *Neural Computation*, 9(8): 1735–1780, 1997.
    - Qifan Huang et al. Flowformer: A flow-based transformer for long sequence modeling. *Proceedings of the International Conference on Learning Representations*, 2022.
    - Kyle Hundman, Valentino Constantinou, Christopher Laporte, Ian Colwell, and Tom Soderstrom. Detecting spacecraft anomalies using lstms and nonparametric dynamic thresholding. In *Proceedings* of the 24th ACM SIGKDD international conference on knowledge discovery & data mining, pp. 387–395, 2018.

- Rob J. Hyndman and George Athanasopoulos. Forecasting: principles and practice. OTexts, 2018.
  - Vincent Jacob, Fei Song, Arnaud Stiegler, Bijan Rad, Yanlei Diao, and Nesime Tatbul. Exathlon: A benchmark for explainable anomaly detection over time series. *Proceedings of the VLDB Endowment*, 14(11):2613–2626, 2021.
  - Yushan Jiang, Kanghui Ning, Zijie Pan, Xuyang Shen, Jingchao Ni, Wenchao Yu, Anderson Schneider, Haifeng Chen, Yuriy Nevmyvaka, and Dongjin Song. Multi-modal time series analysis: A tutorial and survey. *arXiv preprint arXiv:2503.13709*, 2025.
  - Ming Jin, Shiyu Wang, Lintao Ma, Zhixuan Chu, James Y Zhang, Xiaoming Shi, Pin-Yu Chen, Yuxuan Liang, Yuan-Fang Li, Shirui Pan, et al. Time-llm: Time series forecasting by reprogramming large language models. In *The Twelfth International Conference on Learning Representations*, 2024.
  - Taesung Kim, Jinhee Kim, Yunwon Tae, Cheonbok Park, Jangho Choi, and Jaegul Choo. Reversible instance normalization for accurate time-series forecasting against distribution shift. In *International Conference on Learning Representations*, 2022.
  - Nikita Kitaev et al. Reformer: The efficient transformer. In *Proceedings of the International Conference on Learning Representations*, 2020.
  - Takeshi Kojima, Shixiang Shane Gu, Machel Reid, Yutaka Matsuo, and Yusuke Iwasawa. Large language models are zero-shot reasoners. *Advances in neural information processing systems*, 35: 22199–22213, 2022.
  - Yaxuan Kong, Yiyuan Yang, Shiyu Wang, Chenghao Liu, Yuxuan Liang, Ming Jin, Stefan Zohren, Dan Pei, Yan Liu, and Qingsong Wen. Position: Empowering time series reasoning with multimodal llms. *arXiv preprint arXiv:2502.01477*, 2025.
  - Guokun Lai et al. Lstnet: Modeling long- and short-term temporal patterns with deep neural networks. In *Proceedings of the 41st International ACM SIGIR Conference on Research and Development in Information Retrieval*, pp. 115–124, 2018.
  - Zekun Li, Shiyang Li, and Xifeng Yan. Time series as images: Vision transformer for irregularly sampled time series. *Advances in Neural Information Processing Systems*, 36, 2024.
  - Zijing Liang, Yanjie Xu, Yifan Hong, Penghui Shang, Qi Wang, Qiang Fu, and Ke Liu. A survey of multimodel large language models. In *Proceedings of the 3rd International Conference on Computer, Artificial Intelligence and Control Engineering*, pp. 405–409, 2024.
  - Bryan Lim and Stefan Zohren. Time-series forecasting with deep learning: a survey. *Philosophical Transactions of the Royal Society A*, 379(2194):20200209, 2021.
  - Bryan Lim, Sercan O. Arik, Nicolas Loeff, and Tomas Pfister. Temporal fusion transformers for interpretable multi-horizon time series forecasting. *International Journal of Forecasting*, 37(4): 1748–1764, 2021.
  - Dehong Liu et al. Pyraformer: Low-complexity pyramidal attention for long-range time series modeling and forecasting. In *Proceedings of the International Conference on Learning Representations*, 2021.
  - Haotian Liu, Chunyuan Li, Yuheng Li, and Yong Jae Lee. Improved baselines with visual instruction tuning. In *Proceedings of the IEEE/CVF Conference on Computer Vision and Pattern Recognition*, pp. 26296–26306, 2024a.
  - Haotian Liu, Chunyuan Li, Qingyang Wu, and Yong Jae Lee. Visual instruction tuning. *Advances in neural information processing systems*, 36, 2024b.
  - Qinghua Liu and John Paparrizos. The elephant in the room: Towards a reliable time-series anomaly detection benchmark. *Advances in Neural Information Processing Systems*, 37:108231–108261, 2024.

- Qinghua Liu, Paul Boniol, Themis Palpanas, and John Paparrizos. Time-series anomaly detection: Overview and new trends. *Proceedings of the VLDB Endowment (PVLDB)*, 17(12):4229–4232, 2024c.
  - Qinghua Liu, Seunghak Lee, and John Paparrizos. Tsb-autoad: Towards automated solutions for time-series anomaly detection. *Proceedings of the VLDB Endowment*, 18(11):4364–4379, 2025.
  - Qingsong Liu et al. Nonstationary transformer: A transformer model for time-series forecasting. *Proceedings of the 36th AAAI Conference on Artificial Intelligence*, 2022.
  - Xu Liu, Junfeng Hu, Yuan Li, Shizhe Diao, Yuxuan Liang, Bryan Hooi, and Roger Zimmermann. Unitime: A language-empowered unified model for cross-domain time series forecasting. In *Proceedings of the ACM Web Conference 2024*, pp. 4095–4106, 2024d.
  - Yong Liu, Tengge Hu, Haoran Zhang, Haixu Wu, Shiyu Wang, Lintao Ma, and Mingsheng Long. itransformer: Inverted transformers are effective for time series forecasting. *arXiv* preprint *arXiv*:2310.06625, 2023.
  - Yong Liu, Guo Qin, Xiangdong Huang, Jianmin Wang, and Mingsheng Long. Autotimes: Autoregressive time series forecasters via large language models. *Advances in Neural Information Processing Systems*, 37:122154–122184, 2024e.
  - Ilya Loshchilov, Frank Hutter, et al. Fixing weight decay regularization in adam. *arXiv preprint arXiv:1711.05101*, 5:5, 2017.
  - Kevin Lu, Aditya Grover, Pieter Abbeel, and Igor Mordatch. Frozen pretrained transformers as universal computation engines. *Proceedings of the AAAI Conference on Artificial Intelligence*, 36 (7):7628–7636, Jun. 2022.
  - Ganapathy Mahalakshmi, S Sridevi, and Shyamsundar Rajaram. A survey on forecasting of time series data. In 2016 international conference on computing technologies and intelligent data engineering (ICCTIDE'16), pp. 1–8. IEEE, 2016.
  - Pankaj Malhotra, Lovekesh Vig, Gautam Shroff, Puneet Agarwal, et al. Long short term memory networks for anomaly detection in time series. In *Esann*, volume 2015, pp. 89, 2015.
  - Aditya Mathur and Nils Ole Tippenhauer. Swat: A water treatment testbed for research and training on ics security. In 2016 International Workshop on Cyber-physical Systems for Smart Water Networks (CySWater), pp. 31–36. IEEE, 2016.
  - Shentong Mo and Pedro Morgado. Unveiling the power of audio-visual early fusion transformers with dense interactions through masked modeling. In *Proceedings of the IEEE/CVF Conference on Computer Vision and Pattern Recognition*, pp. 27186–27196, 2024.
  - Steffen Moritz, Frederik Rehbach, Sowmya Chandrasekaran, Margarita Rebolledo, and Thomas Bartz-Beielstein. Gecco industrial challenge 2018 dataset: A water quality dataset for the 'internet of things: Online anomaly detection for drinking water quality' competition at the genetic and evolutionary computation conference 2018, kyoto, japan. *Kyoto, Japan*, 2018.
  - Mohsin Munir, Shoaib Ahmed Siddiqui, Andreas Dengel, and Sheraz Ahmed. Deepant: A deep learning approach for unsupervised anomaly detection in time series. *Ieee Access*, 7:1991–2005, 2018.
  - Jingchao Ni, Ziming Zhao, Cheng Ao Shen, Hanghang Tong, Dongjin Song, Wei Cheng, Dongsheng Luo, and Haifeng Chen. Harnessing vision models for time series analysis: A survey. *arXiv* preprint arXiv:2502.08869, 2025.
  - Yuqi Nie, Nam H Nguyen, Phanwadee Sinthong, and Jayant Kalagnanam. A time series is worth 64 words: Long-term forecasting with transformers. In *The Eleventh International Conference on Learning Representations*, 2022.
  - John Paparrizos, Paul Boniol, Themis Palpanas, Ruey S Tsay, Aaron Elmore, and Michael J Franklin. Volume under the surface: a new accuracy evaluation measure for time-series anomaly detection. *Proceedings of the VLDB Endowment*, 15(11):2774–2787, 2022.

- Xiangfei Qiu, Hanyin Cheng, Xingjian Wu, Jilin Hu, Chenjuan Guo, and Bin Yang. A comprehensive survey of deep learning for multivariate time series forecasting: A channel strategy perspective. *arXiv* preprint arXiv:2502.10721, 2025.
  - Alec Radford, Jeff Wu, Rewon Child, David Luan, Dario Amodei, and Ilya Sutskever. Language models are unsupervised multitask learners. 2019. URL https://api.semanticscholar.org/CorpusID:160025533.
  - Alec Radford, Jong Wook Kim, Chris Hallacy, Aditya Ramesh, Gabriel Goh, Sandhini Agarwal, Girish Sastry, Amanda Askell, Pamela Mishkin, Jack Clark, et al. Learning transferable visual models from natural language supervision. In *International conference on machine learning*, pp. 8748–8763. PmLR, 2021.
  - Daniel Roggen, Alberto Calatroni, Mirco Rossi, Thomas Holleczek, Kilian Förster, Gerhard Tröster, Paul Lukowicz, David Bannach, Gerald Pirkl, Alois Ferscha, et al. Collecting complex activity datasets in highly rich networked sensor environments. In 2010 Seventh international conference on networked sensing systems (INSS), pp. 233–240. IEEE, 2010.
  - Peter J Rousseeuw and Katrien Van Driessen. A fast algorithm for the minimum covariance determinant estimator. *Technometrics*, 41(3):212–223, 1999.
  - Mayu Sakurada and Takehisa Yairi. Anomaly detection using autoencoders with nonlinear dimensionality reduction. In *Proceedings of the MLSDA 2014 2nd workshop on machine learning for sensory data analysis*, pp. 4–11, 2014.
  - Bernhard Schölkopf, Robert C Williamson, Alex Smola, John Shawe-Taylor, and John Platt. Support vector method for novelty detection. *Advances in neural information processing systems*, 12, 1999.
  - Iman Sharafaldin, Arash Habibi Lashkari, Ali A Ghorbani, et al. Toward generating a new intrusion detection dataset and intrusion traffic characterization. *ICISSp*, 1:108–116, 2018.
  - Ya Su, Youjian Zhao, Chenhao Niu, Rong Liu, Wei Sun, and Dan Pei. Robust anomaly detection for multivariate time series through stochastic recurrent neural network. In *Proceedings of the 25th ACM SIGKDD international conference on knowledge discovery & data mining*, pp. 2828–2837, 2019.
  - Mingtian Tan, Mike Merrill, Vinayak Gupta, Tim Althoff, and Tom Hartvigsen. Are language models actually useful for time series forecasting? *Advances in Neural Information Processing Systems*, 37:60162–60191, 2024.
  - Hugo Touvron, Louis Martin, Kevin Stone, Peter Albert, Amjad Almahairi, Yasmine Babaei, Nikolay Bashlykov, Soumya Batra, Prajjwal Bhargava, Shruti Bhosale, et al. Llama 2: Open foundation and fine-tuned chat models. *arXiv preprint arXiv:2307.09288*, 2023.
  - Ashish Vaswani, Noam Shazeer, Niki Parmar, Jakob Uszkoreit, Llion Jones, Aidan N Gomez, Łukasz Kaiser, and Illia Polosukhin. Attention is all you need. In *Proceedings of the 31st International Conference on Neural Information Processing Systems*, pp. 6000–6010, 2017.
  - Alexander von Birgelen and Oliver Niggemann. Anomaly detection and localization for cyber-physical production systems with self-organizing maps. *IMPROVE-Innovative Modelling Approaches for Production Systems to Raise Validatable Efficiency: Intelligent Methods for the Factory of the Future*, pp. 55–71, 2018.
  - Yihe Wang, Nan Huang, Taida Li, Yujun Yan, and Xiang Zhang. Medformer: A multi-granularity patching transformer for medical time-series classification. *Advances in Neural Information Processing Systems*, 37:36314–36341, 2024.
  - Qingsong Wen, Tian Zhou, Chaoli Zhang, Weiqi Chen, Ziqing Ma, Junchi Yan, and Liang Sun. Transformers in time series: A survey. *arXiv preprint arXiv:2202.07125*, 2022.
  - Gerald Woo, Chenghao Liu, Akshat Kumar, Caiming Xiong, Silvio Savarese, and Doyen Sahoo. Unified training of universal time series forecasting transformers. In *International Conference on Machine Learning*, pp. 53140–53164. PMLR, 2024.

- Jiyang Woo et al. Etsformer: Exponential smoothing transformers for time-series forecasting.

  Advances in Neural Information Processing Systems, 2022.
  - Haixu Wu et al. Autoformer: Decomposition transformers with auto-correlation for long-term series forecasting. In *Advances in Neural Information Processing Systems*, 2021.
  - Renjie Wu and Eamonn J Keogh. Current time series anomaly detection benchmarks are flawed and are creating the illusion of progress. *IEEE transactions on knowledge and data engineering*, 35(3): 2421–2429, 2021.
  - Zonghan Wu, Shirui Pan, Guodong Long, Jing Jiang, Xiaojun Chang, and Chengqi Zhang. Connecting the dots: Multivariate time series forecasting with graph neural networks. In *Proceedings of the 26th ACM SIGKDD international conference on knowledge discovery & data mining*, pp. 753–763, 2020.
  - Zonghan Wu et al. Timesnet: A pre-trained temporal model for time series forecasting. *arXiv preprint arXiv:2301.03461*, 2023.
  - Lili Xu, Martin Herold, Nandin-Erdene Tsendbazar, Dainius Masiliūnas, Linlin Li, Myroslava Lesiv, Steffen Fritz, and Jan Verbesselt. Time series analysis for global land cover change monitoring: A comparison across sensors. *Remote Sensing of Environment*, 271:112905, 2022.
  - Takehisa Yairi, Yoshikiyo Kato, and Koichi Hori. Fault detection by mining association rules from house-keeping data. In *proceedings of the 6th International Symposium on Artificial Intelligence, Robotics and Automation in Space*, volume 18, pp. 21. Citeseer, 2001.
  - An Yang, Baosong Yang, Beichen Zhang, Binyuan Hui, Bo Zheng, Bowen Yu, Chengyuan Li, Dayiheng Liu, Fei Huang, Haoran Wei, Huan Lin, Jian Yang, et al. Qwen2.5 technical report. arXiv preprint arXiv:2412.15115, 2024.
  - Chin-Chia Michael Yeh, Yan Zhu, Liudmila Ulanova, Nurjahan Begum, Yifei Ding, Hoang Anh Dau, Diego Furtado Silva, Abdullah Mueen, and Eamonn Keogh. Matrix profile i: all pairs similarity joins for time series: a unifying view that includes motifs, discords and shapelets. In *2016 IEEE 16th international conference on data mining (ICDM)*, pp. 1317–1322. Ieee, 2016.
  - Yuyang Zeng et al. Dlinear: Decoupled linear models for accurate forecasting. *Proceedings of the 10th International Conference on Learning Representations*, 2023.
  - Haibo Zhang et al. Lightts: Lightweight time series modeling with mlp. *arXiv preprint* arXiv:2208.07933, 2022.
  - Jingyi Zhang, Jiaxing Huang, Sheng Jin, and Shijian Lu. Vision-language models for vision tasks: A survey. *IEEE Trans. Pattern Anal. Mach. Intell.*, 46(8):5625–5644, February 2024. ISSN 0162-8828.
  - Siru Zhong, Weilin Ruan, Ming Jin, Huan Li, Qingsong Wen, and Yuxuan Liang. Time-vlm: Exploring multimodal vision-language models for augmented time series forecasting. 2025.
  - Haoyi Zhou et al. Informer: Beyond efficient transformer for long sequence time-series forecasting. In *Proceedings of the AAAI Conference on Artificial Intelligence*, volume 35, pp. 11106–11115, 2021.
  - Tian Zhou, Peisong Niu, Liang Sun, Rong Jin, et al. One fits all: Power general time series analysis by pretrained lm. *Advances in neural information processing systems*, 36:43322–43355, 2023.
  - Tian Zhou et al. Fedformer: Frequency enhanced decomposed transformer for long-term series forecasting. In *Proceedings of the International Conference on Machine Learning*, pp. 27268–27286, 2022.
  - Jiaxin Zhuang, Leon Yan, Zhenwei Zhang, Ruiqi Wang, Jiawei Zhang, and Yuantao Gu. See it, think it, sorted: Large multimodal models are few-shot time series anomaly analyzers. *arXiv preprint arXiv:2411.02465*, 2024.

# SUPPLEMENTARY MATERIAL FOR MLLM4TS

# A EXPERIMENTAL SETUP

#### A.1 DATASET DESCRIPTION

We evaluate MLLM4TS on standard time-series analysis tasks using widely adopted benchmark datasets. For classification and forecasting, we follow the data processing and train-validation-test split protocols established in TimesNet (Wu et al., 2023). For anomaly detection, we use the recent TSB-AD benchmark (Liu & Paparrizos, 2024; Liu et al., 2025), which addresses common concerns regarding the quality and reliability of time-series anomaly detection datasets. Detailed dataset statistics are provided in Table 5 (classification), Table 6 (anomaly detection), and Table 7 (forecasting).

Table 5: Summary of datasets used for the time-series classification task from UEA archive (Bagnall et al., 2018). The table includes the number of training and test samples, sequence length, number of time series dimensions, number of classes, and data type for each dataset. These datasets span various domains such as sensor readings, EEG, audio, and speech, providing a diverse evaluation for time-series classification.

Dataset	Train	Test	Len	Dim	Class	Domain
EC	261	263	1751	3	4	SPECTRO
FD	5890	3524	62	144	2	EEG
HW	150	850	152	3	26	HAR
НВ	204	205	405	61	2	AUDIO
JV	270	370	29	12	9	AUDIO
PSF	267	173	144	963	7	OTHER
SRSCP1	268	293	896	6	2	EEG
SRSCP2	200	180	1152	7	2	EEG
SAD	6599	2199	93	13	10	SPEECH
UWGL	2238	2241	315	3	8	HAR

Table 6: Summary of datasets used for the time-series anomaly detection task on TSB-AD benchmark (Liu & Paparrizos, 2024). The 'Anomaly Type' column indicates whether the datasets feature point anomalies (P) or sequence anomalies (Seq).

Domain	Dataset	# TS	Avg Dim	Avg TS Len	Avg # Anomaly	Avg Anomaly Len	Anomaly Ratio	Anomaly Type
	GHL (2016)	25	19	199001.0	2.2	1035.2	1.1%	Seq
	Genesis (2018)	1	18	16220.0	3.0	16.7	0.3%	Seq
	SWaT (2016)	2	59	207457.5	16.5	1093.6	12.7%	Seq
Sensor	SMAP (2018)	27	25	7855.9	1.3	196.3	2.9%	Seq
	MSL (2018)	16	55	3119.4	1.3	111.7	5.1%	Seq
	GECCO (2018)	1	9	138521.0	51.0	33.8	1.2%	Seq
	CATSv2 (2023)	6	17	240000.0	11.5	811.6	3.7%	Seq
I Ivanon A otivity	Daphnet (2009)	1	9	38774.0	6.0	384.3	5.9%	Seq
HumanActivity	OPP (2010)	8	248	17426.8	1.4	394.3	4.1%	Seq
	Exathlon (2021)	27	21	60878.4	4.3	1373.3	9.8%	Seq
Facility	SMD (2019)	22	38	25466.4	8.9	112.8	3.8%	Seq
	PSM (2021)	1	25	217624.0	72.0	338.6	11.2%	P&Seq
Finance	CreditCard (2018)	1	29	284807.0	465.0	1.1	0.2%	P&Seq
	MITDB (2000)	13	2	336153.8	15.2	1846.8	2.7%	Seq
Medical	SVDB (1990)	31	2	207122.6	68.3	268.2	4.8%	Seq
	LTDB (2000)	5	2	100000.0	105.0	134.4	15.5%	Seq
Environment	TAO (2006)	13	3	10000.0	788.2	1.1	8.7%	P&Seq

Table 7: Summary of datasets used for the time-series forecasting task. 'Dim' denotes the variate number. 'Dataset Size' denotes the total number of time points in (Train, Validation, Test) splits respectively. 'Forecast Length' denotes the future time points to be predicted. 'Frequency' denotes the sampling interval of time points.

Dataset	Dim	Forecast Length	Dataset Size	Frequency	Domain
Weather (2021)	21	{96, 192, 336, 720}	(36792, 5271, 10540)	10min	Weather
Solar-Energy (2023)	137	{96, 192, 336, 720}	(36601, 5161, 10417)	10min	Energy
ETTh1 (2021)	7	{96, 192, 336, 720}	(8545, 2881, 2881)	Hourly	Electricity
ECL (2021)	321	{96, 192, 336, 720}	(18317, 2633, 5261)	Hourly	Electricity
Traffic (2021)	862	{96, 192, 336, 720}	(12185, 1757, 3509)	Hourly	Transportation

# A.2 IMPLEMENTATION DETAILS

MLLM4TS converts multivariate time series into a single composite image by plotting each channel as a color-coded line within a horizontally arranged layout. The pseudo-code for this transformation is provided in Algorithm 1, where the resulting image tensor  $\hat{I} \in \mathbb{R}^{3 \times H \times W}$  is generated from the input time-series sequence  $\mathbf{X} = \{\mathbf{x}_t\}_{t=1}^L \in \mathbb{R}^{L \times C}$  and subsequently used in the core model processing.

We present the core processing pipeline of MLLM4TS in Algorithm 2. The image tensor and the original time series are fed into the vision encoder and the time-series tokenization module, respectively, where the latter includes patching and linear projection. The resulting visual and temporal embeddings are aligned using the proposed temporal-aware strategy and subsequently fused before being passed to the language model backbone. The final prediction is obtained via a task-specific linear head on the last-layer hidden states as illustrated in Algorithm 3. For classification, we supervise the predicted logits  $\mathbf{Y}_{\text{cls}} \in \mathbb{R}^{B \times K}$  with one-hot labels  $\mathbf{Y}^* \in \{0,1\}^{B \times K}$  via the cross-entropy loss  $\mathcal{L}_{\text{cls}} = -\frac{1}{B} \sum_{i=1}^{K} \sum_{k=1}^{K} Y_{i,k}^* \log \left[ \operatorname{softmax}(\mathbf{Y}_{\text{cls},i}) \right]_k$ . For anomaly detection, we reconstruct the input time series  $\mathbf{X} \in \mathbb{R}^{B \times L \times C}$  and minimize the mean-squared error  $\mathcal{L}_{\text{ad}} = \|\mathbf{Y}_{\text{ad}} - \mathbf{X}\|^2$ . The anomaly score is obtained via the reconstruction loss between the original and reconstructed time series. For forecasting, we predict the future series  $\mathbf{X}_{L+1:L+F} \in \mathbb{R}^{B \times F \times C}$  and likewise minimize  $\mathcal{L}_{\text{fc}} = \|\mathbf{Y}_{\text{fc}} - \mathbf{X}_{L+1:L+F}\|^2$ . To handle varying numbers of input channels and enhance generalization, we adopt a cross-channel weight sharing strategy, which implicitly captures inter-variable dependencies during training (Nie et al., 2022). This mechanism complements the visual embeddings that also encode cross-channel relationships.

At the core of MLLM4TS are two pretrained backbones: the vision encoder CLIP-ViT-L-14 (Radford et al., 2021) and the language model GPT-2 (Radford et al., 2019), which are used by default unless stated otherwise. All experiments are conducted using PyTorch on NVIDIA A100 GPUs. We adopt the AdamW optimizer (Loshchilov et al., 2017) with a cosine learning rate scheduler and a warm-up starting at  $10^{-6}$ . Classification is trained for a maximum of 50 epochs with early stopping patience of 15, while anomaly detection and forecasting use a maximum of 10 epochs with patience set to 3. Trainable projection layers and output heads are implemented as linear layers for simplicity and efficiency. All results are averaged over five runs with different random seeds. Performance stability is illustrated in Figure 7, which includes error bars representing standard deviation.

# B SUPPLEMENTARY RESULTS

In this section, we present supplementary evaluation results for MLLM4TS and baseline methods. Section B.1 provides performance variability illustrated with error bars, followed by comprehensive results for the mainstream time-series analysis tasks in Section B.2. Detailed ablation study results are reported in Section B.3.

965

966

967

19:  $\mathbf{Z} \leftarrow \mathbf{V} + \mathbf{T}'$ 

21: return F

20:  $\mathbf{F} \leftarrow \text{LanguageModel}(\mathbf{Z}) \in \mathbb{R}^{B \times N_{\text{ts}} \times d}$ 

```
921
               Algorithm 1 Time Series to Image
922
               Require: Input time series \mathbf{X} = \{\mathbf{x}_t\}_{t=1}^L \in \mathbb{R}^{L \times C}, image size (H, W)
923
924
               Ensure: Image tensor \hat{I} \in \mathbb{R}^{3 \times H \times W}
925
                 1: G \leftarrow (C, 1)
                                                                                                                                                   \triangleright grid rows = channels
926
                 2: colors \leftarrow colormap(C)
927
                 3: for c = \{1, \dots, C\} do
                            \mathbf{x}^i \leftarrow \mathbf{X}_{:,i}
                 4:
                                                                                                                                                      ⊳ extract i-th channel
928
                 5:
                            Create subplot in row i of grid G
929
                            plot(1: L, \mathbf{x}^i) in color colors[c]
                 6:
930
                 7: end for
931
                 8: Render the figure to an image tensor I
932
                 9: return \hat{I}
933
934
936
937
938
939
940
941
               Algorithm 2 MLLM4TS Backbone
942
               Require: Time series \mathbf{x}_{1:L} \in \mathbb{R}^{L \times C}, image tensor \hat{I} \in \mathbb{R}^{3 \times H \times W}
943
               Ensure: Fused multi-modal token features \mathbf{F} \in \mathbb{R}^{B \times N_{ts} \times d}, where d is the feature dimension of
944
945
                      language model
946
                 1: Plot Embedding:
947
                 2: \mathbf{V} \leftarrow \text{VisionEncoder}(\hat{I}) \in \mathbb{R}^{B \times N_{\text{vis}} \times d_v}
                                                                                                                         \triangleright reshape V \in \mathbb{R}^{d_v \times (B N_{\text{vis}})} if needed
948
                 3: \mathbf{V}' \leftarrow W_{\text{proj}} \mathbf{V} + b_{\text{proj}} \in \mathbb{R}^{B \times N_{\text{vis}} \times d}
                                                                                                                                 \triangleright Plot Projection W_{\text{proj}} \in \mathbb{R}^{d \times d_v}
949
                 4: Time Series Embedding:
950
                 5: \mu \leftarrow \text{mean}(\mathbf{x}_{1:L}, \text{dim} = 1) \in \mathbb{R}^{B \times 1 \times C}
951
                 6: \sigma \leftarrow \sqrt{\text{var}(\mathbf{x}_{1:L}, \text{dim} = 1) + \epsilon} \in \mathbb{R}^{B \times 1 \times C}
952
                 7: \mathbf{x} \leftarrow (\mathbf{x}_{1:L} - \mu) / \sigma
                                                                                                                                         ▶ Time Series Normalization
953
                 8: \mathbf{X} \leftarrow \operatorname{transpose}(\mathbf{x}_{1:L}, (B, L, C) \rightarrow (B, C, L))
954
                 9: \tilde{\mathbf{X}} \leftarrow \text{Padding}(\tilde{\mathbf{X}}) \in \mathbb{R}^{B \times C \times L'}
955
               10: \hat{\mathbf{X}} \leftarrow \text{Unfold}(\tilde{\mathbf{X}}, P_{ts}, S) \in \mathbb{R}^{B \times C \times N_{ts} \times P_{ts}}
                                                                                                          \triangleright Patch size P_{ts} = L/r detailed in Section 3.2
956
               11: \mathbf{T} \leftarrow \text{reshape}(\hat{\mathbf{X}}, (B, N_{\text{ts}}, P_{ts} C))
12: \mathbf{T}' \leftarrow W_{\text{tok}} \mathbf{T} + b_{\text{tok}} \in \mathbb{R}^{B \times N_{\text{ts}} \times d}
957
                                                                                                                  \triangleright Time Series Tokenizer W_{\mathrm{tok}} \in \mathbb{R}^{d \times P_{ts}C}
958
959
               13: Cross-modal Alignment:
960
               14: H = W = |\sqrt{N_{\text{vis}}}|
961
               15: V \leftarrow \text{reshape}(\text{transpose}(\mathbf{V}', 1, 2), (B, d, H, W))
962
               16: \bar{\mathbf{V}} \leftarrow \operatorname{mean_H}(\mathcal{V}) \in \mathbb{R}^{B \times d \times W}

    Average-pool across the height (H) dimension

963
               17: \widetilde{\mathbf{V}} \leftarrow \operatorname{interp}(\bar{\mathbf{V}}, N_{\mathrm{ts}}) \in \mathbb{R}^{B \times N_{\mathrm{ts}} \times d}
                                                                                                                                                     964
               18: Fusion & decoding:
```

# Algorithm 3 Task-Specific Head

**Require:** Final hidden states  $\mathbf{F} \in \mathbb{R}^{B \times N \times d}$ , mean  $\boldsymbol{\mu} \in \mathbb{R}^{B \times 1 \times C}$ , std. dev.  $\boldsymbol{\sigma} \in \mathbb{R}^{B \times 1 \times C}$  from Algorithm 2

# Ensure: Task outputs Y

- 1: Classification head:
- 2:  $\mathbf{u} \leftarrow \text{Pooling}(\mathbf{F}) \in \mathbb{R}^{B \times d}$
- 3:  $\mathbf{u}' \leftarrow \text{LayerNorm}(\mathbf{u})$
- 4:  $\mathbf{Y}_{\mathrm{cls}} \leftarrow W_{\mathrm{cls}} \, \mathbf{u}' + b_{\mathrm{cls}} \in \mathbb{R}^{B \times K}$

 $\quad \triangleright \ Classification \ logits$ 

- 5: Anomaly detection head:
- 6:  $\mathbf{G} \leftarrow \text{LayerNorm}(\mathbf{F}) \in \mathbb{R}^{B \times L \times d}$

 $\triangleright L = N$  in anomaly detection

- 7:  $\mathbf{R} \leftarrow W_{\mathrm{ad}} \mathbf{G} + b_{\mathrm{ad}} \in \mathbb{R}^{B \times L \times C}$
- 8:  $\mathbf{Y}_{\mathrm{ad}} \leftarrow \mathbf{R} \times \boldsymbol{\sigma} + \boldsymbol{\mu}$

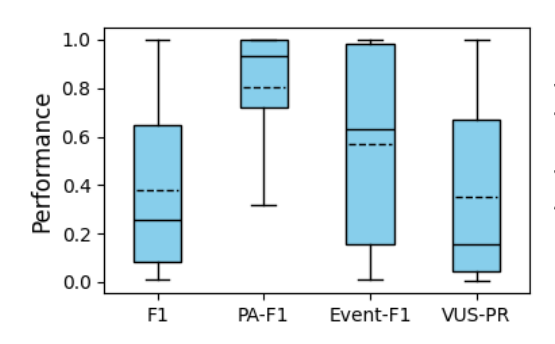
> Reconstructed time series

- 9: Forecasting head:
- 10:  $\mathbf{H} \leftarrow \text{LayerNorm}(\mathbf{F}) \in \mathbb{R}^{(B \times C) \times (N \times d)} \triangleright \text{Cross-channel weight sharing mechanism (Nie et al., 2022)}$
- 11:  $\mathbf{P} \leftarrow W_{\mathrm{fc}} \mathbf{H} + b_{\mathrm{fc}} \in \mathbb{R}^{(B \times C) \times F}$
- 12:  $\mathbf{P}' \leftarrow \text{reshape}(\mathbf{P}, (B, C, F))$
- 13:  $\mathbf{Y}_{\mathrm{fc}} \leftarrow \mathbf{P}' \times \boldsymbol{\sigma} + \boldsymbol{\mu}$
- 14: return  $\{Y_{cls}, Y_{ad}, Y_{fc}\}$

▶ Predicted time series

#### B.1 ERROR BARS

We report the performance standard deviation of MLLM4TS across five random seeds in Figure 7, based on four evaluation measures available in the TSB-AD benchmark (Liu & Paparrizos, 2024). The consistently low standard deviation across all metrics suggests that MLLM4TS exhibits stable and reliable performance.



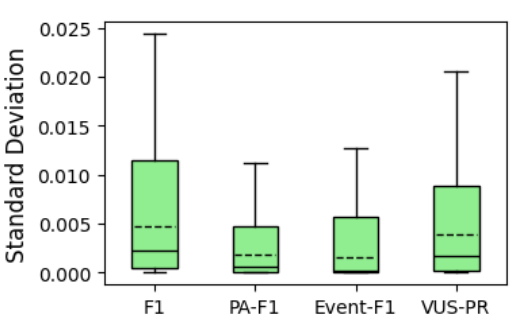


Figure 7: Distribution of standard deviation of four evaluation measures for time-series anomaly detection task on TSB-AD benchmark (comprising 180 time series). Results come from five random seeds. The mean is marked by a dashed line and the median by a solid line.

# B.2 FULL TIME-SERIES ANALYSIS RESULTS

We provide complete evaluation results for time-series classification in Table 8, anomaly detection in Table 9, 10, forecasting in Table 11, few-shot learning in Table 12 and zero-shot learning in Table 13.

# **B.3** ABLATION STUDY RESULTS

We present ablation studies across multiple aspects of different time-series analysis tasks, including classification (Table 14), anomaly detection (Table 15), and forecasting (Table 16). In addition, Figure 8 illustrates the effect of different language model backbones, while Table 17 reports the impact of dimensionality reduction during plotting.

Table 8: Performance overview on the classification task on UEA datasets (Bagnall et al., 2018). \*. in the Transformers indicates the name of \*former. The best performance is highlighted in **bold**, and the second-best is underlined.

Category	Model	EC	FD	HW	HB	JV	PSF	SRSCP1	SRSCP2	SAD	UWGL	Average
Classical	XGBoost (2016)	43.7	63.3	15.8	73.2	86.5	98.3	84.6	48.9	69.6	75.9	66.0
Classical	Rocket (2020)	45.2	64.7	58.8	75.6	96.2	75.1	90.8	53.3	71.2	94.4	72.5
RNN	LSTNet (2018)	39.9	65.7	25.8	77.1	98.1	86.7	84.0	52.8	100.0	87.8	71.8
KININ	LSSL (2021)	31.1	66.7	24.6	72.7	98.4	86.1	90.8	52.2	100.0	85.9	70.9
CNN	TCN (2019)	28.9	52.8	53.3	75.6	98.9	68.8	84.6	55.6	95.6	88.4	70.3
CIVIV	TimesNet (2023)	35.7	68.6	32.1	78.0	98.4	89.6	91.8	57.2	99.0	85.3	73.6
	Trans. (2017)	32.7	67.3	32.0	76.1	98.7	82.1	92.2	53.9	98.4	85.6	71.9
	Re. (2020)	31.9	68.6	27.4	77.1	97.8	82.7	90.4	56.7	97.0	85.6	71.5
	In. (2021)	31.6	67.0	32.8	80.5	98.9	81.5	90.1	53.3	100.0	85.6	72.1
	Pyra. (2021)	30.8	65.7	29.4	75.6	98.4	83.2	88.1	53.3	99.6	83.4	70.8
Transformers	Auto. (2021)	31.6	68.4	36.7	74.6	96.2	82.7	84.0	50.6	100.0	85.9	71.1
	Station. (2022)	32.7	68.0	31.6	73.7	99.2	87.3	89.4	57.2	100.0	87.5	72.7
	FED. (2022)	31.2	66.0	28.0	73.7	98.4	80.9	88.7	54.4	100.0	85.3	70.7
	ETS. (2022)	28.1	66.3	32.5	71.2	95.9	86.0	89.6	55.0	100.0	85.0	71.0
	Flow. (2022)	33.8	67.6	33.8	77.6	98.9	83.8	92.5	56.1	98.8	86.6	73.0
MLP	DLinear (2023)	32.6	68.0	27.0	75.1	96.2	75.1	87.3	50.5	81.4	82.1	67.5
MLP	LightTS (2022)	29.7	67.5	26.1	75.1	96.2	88.4	89.8	51.1	100.0	80.3	70.4
	MOMENT (2024)	35.7	63.3	30.8	72.2	71.6	89.6	84.0	47.8	98.1	90.9	68.4
FM	UniTS (2024)	37.6	70.5	29.7	80.0	97.8	93.1	93.9	61.1	98.9	87.8	75.0
ΓIVI	OFA (2023)	33.1	69.2	30.9	78.0	82.4	87.9	93.5	60.1	99.3	86.9	72.2
	MLLM4TS(Ours)	38.8	68.5	40.0	80.0	99.7	<u>94.2</u>	93.2	<u>60.6</u>	<u>99.6</u>	<u>92.8</u>	76.7

Table 9: Performance overview on the anomaly detection task on TSB-AD-M benchmark (Liu & Paparrizos, 2024). Performance is evaluated in VUS-PR (Paparrizos et al., 2022; Boniol et al., 2025). The best performance is highlighted in **bold**, and the second-best is <u>underlined</u>.

Dataset		S	tatistical					NN				FM
	PCA (2017)	KMeansAD (2001)	CBLOF (2003)	MCD (1999)	OCSVM (1999)	CNN (2018)	OmniAnomaly (2019)	LSTMAD (2015)	USAD (2020)	AutoEncoder (2014)	OFA (2023)	MLLM4TS (Ours)
GHL	0.012	0.030	0.019	0.014	0.036	0.062	0.065	0.062	0.065	0.047	0.007	0.007
Genesis	0.019	0.891	0.024	0.059	0.076	0.100	0.003	0.037	0.003	0.007	0.013	0.017
SWaT	0.449	0.159	0.292	0.538	0.444	0.150	0.150	0.156	0.150	0.575	0.139	0.183
SMAP	0.093	0.380	0.137	0.104	0.116	0.193	0.124	0.163	0.108	0.129	0.208	0.348
MSL	0.149	0.435	0.215	0.229	0.216	0.217	0.217	0.217	0.226	0.219	0.212	0.237
GECCO	0.202	0.055	0.034	0.033	0.038	0.303	0.021	0.019	0.021	0.049	0.000	0.712
CATSv2	0.118	0.117	0.059	0.132	0.080	0.080	0.041	0.041	0.041	0.063	0.049	0.105
Daphnet	0.130	0.297	0.096	0.135	0.064	0.203	0.340	0.311	0.340	0.129	0.378	0.338
OPP	0.299	0.063	0.143	0.167	0.121	0.177	0.177	0.165	0.177	0.144	0.072	0.091
Exathlon	0.949	0.372	0.857	0.796	0.830	0.684	0.839	0.816	0.839	0.909	0.865	0.879
SMD	0.364	0.358	0.223	0.260	0.285	0.174	0.325	0.325	0.160	0.301	0.398	0.455
PSM	0.163	0.208	0.194	0.255	0.191	0.236	0.160	0.236	0.194	0.280	0.158	0.145
CreditCard	0.103	0.020	0.032	0.060	0.024	0.022	0.021	0.022	0.021	0.028	0.156	0.143
MITDB	0.065	0.063	0.039	0.037	0.038	0.115	0.092	0.092	0.118	0.038	0.032	0.112
SVDB	0.112	0.203	0.068	0.067	0.065	0.352	0.155	0.155	0.322	0.065	0.096	0.117
LTDB	0.244	0.414	0.202	0.214	0.198	0.303	0.444	0.303	0.411	0.206	0.134	0.287
TAO	1.000	0.862	1.000	1.000	0.810	0.991	0.813	0.991	0.813	0.997	0.909	1.000
TSB-AD-M	0.310	0.295	0.273	0.271	0.265	0.312	0.312	0.307	0.304	0.295	0.296	0.349

Table 10: Performance overview on the anomaly detection task on four common datasets. Performance is evaluated in point-adjusted F-score. The best performance is highlighted in **bold**, and the second-best is <u>underlined</u>.

Dataset	MLLM4TS (Ours)	OFA (2023)	TimesNet (2023)	PatchTS. (2022)	ETS. (2022)	FED. (2022)	LightTS (2022)	DLinear (2023)	Station. (2022)	Auto. (2021)	Pyra. (2021)	In. (2021)	Re. (2020)	Trans. (2017)
SMD	87.4	86.9	84.6	84.6	83.1	85.1	82.5	77.1	84.7	85.1	83.0	81.7	75.3	79.6
MSL	90.8	81.8	81.8	78.7	85.0	78.6	79.0	84.9	77.5	79.1	84.9	84.1	84.4	78.7
SMAP	78.4	68.8	69.4	68.8	69.5	70.8	69.2	69.3	71.1	71.1	71.1	69.9	70.4	69.7
SWaT	95.5	95.1	93.0	85.7	84.9	93.2	93.3	87.5	79.9	92.7	91.8	81.4	82.8	80.4
PSM	97.6	97.1	<u>97.3</u>	96.1	91.8	97.2	97.2	93.6	<u>97.3</u>	93.3	82.1	77.1	73.6	76.1
Average	89.9	85.9	85.2	82.8	82.9	85.0	84.2	82.5	82.1	84.3	82.6	78.8	77.3	76.9

Table 11: Performance overview on the forecasting task. The best performance is highlighted in **bold**, and the second-best is underlined.

96   92   336   720   96   992   336   720   92   336   720   92   720   936	MSE 0.149 0.193 0.243 0.315 0.225 0.167 0.185 0.192 0.209	0.198 0.245 0.282 0.337 0.266 0.231 0.245 0.251 0.257	MSE 0.154 0.196 0.254 0.321 0.231 0.196 0.224 0.240	MAE 0.205 0.245 0.290 0.337 0.269 0.261 0.292	MSE   0.144   0.196   0.265   0.337   0.236   0.213	MAE 0.196 0.243 0.295 0.342 0.269 0.241	MSE 0.158 0.207 0.262 0.342 0.242	MAE 0.208 0.254 0.298 0.353 0.278	MSE 0.149 0.195 0.245 0.318	MAE 0.200 0.243 0.282	MSE 0.180 0.226 0.280	MAE 0.223 0.261	MSE 0.163 0.205	MAE 0.211 0.250	MSE 0.152 0.220	MAE 0.237 0.282	MSE 0.149 0.194	MAE 0.198 0.241	MSE 0.172 0.219	MAE 0.220 0.261
92 336 720 Avg   96 192 336 720	0.193 0.243 0.315 0.225 0.167 0.185 0.192 0.209	0.245 <b>0.282</b> 0.337 0.266 0.231 0.245 0.251	0.196 0.254 0.321 0.231 0.196 0.224	0.245 0.290 0.337 0.269	0.196 0.265 0.337 0.236	0.243 0.295 0.342 0.269	0.207 0.262 0.342	0.254 0.298 0.353	0.195 0.245 0.318	$\frac{0.243}{0.282}$	0.226									
96 192 1336 120	0.167 0.185 0.192 0.209	0.231 0.245 0.251	0.196 0.224	0.261	0.213		0.242		0.227	0.338	0.260	0.300 0.348 0.283	0.254 0.329	0.289 0.340	0.265 0.323	0.319 0.362 0.300	0.245 0.314	0.282 0.334 0.264	0.280 0.365 0.259	0.306 0.359
336	0.192 0.209	0.245 0.251		0.292			0.171	0.221	0.227	0.289	0.200	0.283	0.238	0.272	0.240	0.300	0.226	0.204	0.239	0.287
Avg	0.400	0.207	0.256	0.308 0.321	0.233 0.236 0.241	0.262 0.270 0.289	0.190 0.203 0.222	0.236 0.248 0.262	0.244 0.225 0.243	0.289 0.291 0.301	0.251 0.270 0.271	0.290 0.301 0.298	0.200 0.209 0.213	0.270 0.276 0.276	0.211 0.228 0.236	0.273 0.287 0.295	0.187 0.196 <b>0.205</b>	0.263 0.260 0.269	0.200 0.212 0.211	0.268 0.274 0.273
	0.188	0.246	0.229	0.296	0.231	0.266	0.197	0.242	0.234	0.293	0.254	0.291	0.202	0.269	0.217	0.278	0.189	0.257	0.200	0.268
92 336	0.366 0.404 0.425 0.436	0.400 0.420 0.434 0.467	0.377 0.413 0.436 0.477	0.404 0.424 0.444 0.481	0.343 0.379 0.412 0.458	0.376 0.405 0.423 0.455	0.360 0.391 0.408 0.429	0.397 0.419 0.432 <b>0.452</b>	0.380 0.405 0.422 <u>0.430</u>	0.412 0.422 0.433 0.459	0.386 0.428 0.464 0.473	0.409 0.436 0.456 0.479	0.386 0.422 0.444 0.500	0.405 0.439 0.457 0.498	0.375 0.405 0.439 0.472	0.399 <u>0.416</u> 0.443 0.490	0.370 0.413 0.422 0.447	0.399 0.421 0.436 0.466	0.384 0.557 0.491 0.521	0.402 0.436 0.469 0.500
Avg	0.408	0.430	0.426	0.438	0.398	0.415	0.397	0.425	0.409	0.432	0.438	0.445	0.438	0.450	0.423	0.437	0.413	0.431	0.458	0.450
92 336	0.134 0.153 0.169 0.204	0.232 0.251 0.267 0.295	0.137 0.154 0.169 0.207	0.236 0.251 0.267 0.300	0.126 0.144 0.163 0.195	0.223 0.241 <b>0.255</b> 0.286	0.140 0.159 0.177 0.216	0.236 0.253 0.270 0.303	0.137 0.162 0.175 0.207	0.244 0.271 0.279 0.306	0.171 0.178 0.194 0.232	0.266 0.274 0.289 0.319	0.132 0.153 0.167 0.192	0.227 0.249 0.262 <b>0.285</b>	0.153 0.152 0.169 0.233	0.237 0.249 0.267 0.344	0.129 0.147 <b>0.163</b> 0.197	0.222 0.240 0.259 0.290	0.168 0.184 0.198 0.220	0.272 0.289 0.300 0.320
Avg	0.165	0.261	0.167	0.264	0.157	0.251	0.173	0.266	0.170	0.275	0.194	0.287	0.161	0.256	0.177	0.274	0.159	0.253	0.192	0.295
96	0.378 0.396 0.404	0.268 0.281 0.280 0.304	0.395 0.410 0.414 0.445	0.283 0.290 0.295 0.311	0.356 0.385 0.398 0.439	0.245 0.251 0.262 0.284	0.369 0.394 0.413 0.449	0.257 0.268 0.278 0.299	0.373 0.390 0.407 0.438	0.280 0.288 0.299 0.310	0.438 0.446 0.461 0.494	0.291 0.293 0.300 0.318	0.351 0.364 0.382 0.420	0.257 0.265 0.273 0.292	0.410 0.423 0.436 0.466	0.282 0.287 0.296 0.315	0.360 0.379 0.392 0.432	0.249 0.256 0.264 0.286	0.593 0.617 0.629 0.640	0.321 0.336 0.336 0.350 0.336
12	0   0   0   0   0   0   0   0   0   0	20   0.204 vg   0.165 6   0.378 02   0.396 036   0.404 20   0.446	20         0.204         0.295           vg         0.165         0.261           6         0.378         0.268           02         0.396         0.281           36         0.404         0.280           20         0.446         0.304	20         0.204         0.295         0.207           yg         0.165         0.261         0.167           6         0.378         0.268         0.395           02         0.396         0.281         0.410           06         0.404         0.280         0.414           00         0.446         0.304         0.445	20         0.204         0.295         0.207         0.300           vg         0.165         0.261         0.167         0.264           6         0.378         0.268         0.395         0.283           022         0.396         0.281         0.410         0.290           06         0.404         0.280         0.414         0.295           00         0.446         0.304         0.445         0.311	20         0.204         0.295         0.207         0.300         0.195           yg         0.165         0.261         0.167         0.264         0.157           6         0.378         0.268         0.395         0.283         0.356           02         0.396         0.281         0.410         0.290         0.385           06         0.404         0.280         0.414         0.295         0.398           00         0.446         0.304         0.445         0.311         0.439	20         0.204         0.295         0.207         0.300         0.195         0.286           gg         0.165         0.261         0.167         0.264         0.157         0.251           6         0.378         0.268         0.395         0.283         0.356         0.245           22         0.396         0.281         0.410         0.290         0.385         0.251           16         0.404         0.280         0.414         0.295         0.398         0.261           20         0.446         0.304         0.445         0.311         0.439         0.284	20         0.204         0.295         0.207         0.300         0.195         0.286         0.216           gg         0.165         0.261         0.167         0.264 <b>0.157 0.251</b> 0.173           6         0.378         0.268         0.395         0.283         0.356         0.245         0.394           02         0.396         0.281         0.410         0.290         0.385 <b>0.251</b> 0.394           06         0.404         0.280         0.414         0.295         0.398 <b>0.262</b> 0.413           00         0.446         0.304         0.445         0.311         0.439 <b>0.284</b> 0.449	20         0.204         0.295         0.207         0.300         0.195         0.286         0.216         0.303           yg         0.165         0.261         0.167         0.264 <b>0.157 0.251</b> 0.173         0.266           6         0.378         0.288         0.395         0.233         0.355 <b>0.245</b> 0.369         0.287           02         0.396         0.281         0.410         0.290         0.385 <b>0.257</b> 0.394         0.268           06         0.404         0.280         0.414         0.295         0.398 <b>0.262</b> 0.413         0.278           00         0.446         0.304         0.445         0.311         0.439 <b>0.284</b> 0.449         0.299	20         0.204         0.295         0.207         0.300         0.195         0.286         0.216         0.303         0.207           vg         0.165         0.261         0.167         0.264 <b>0.157 0.251</b> 0.173         0.266         0.170           6         0.378         0.281         0.395         0.233         0.356         0.245         0.369         0.257         0.373           026         0.981         0.401         0.290         0.385 <b>0.251</b> 0.394         0.268         0.390           06         0.404         0.280         0.414         0.295         0.398 <b>0.262</b> 0.413         0.278         0.407           09         0.446         0.304         0.445         0.311         0.439 <b>0.284</b> 0.449         0.299         0.438	20         0.204         0.295         0.207         0.300         0.195         0.286         0.216         0.303         0.207         0.306           gg         0.165         0.261         0.167         0.264         0.157         0.251         0.173         0.266         0.170         0.275           6         0.378         0.288         0.395         0.283         0.356         0.245         0.369         0.257         0.373         0.280           02         0.396         0.281         0.410         0.290         0.385         0.245         0.394         0.268         0.390         0.286           06         0.404         0.280         0.414         0.295         0.398         0.262         0.413         0.278         0.407         0.299           01         0.446         0.304         0.445         0.311         0.439         0.284         0.449         0.299         0.438         0.310	20         0.204         0.295         0.207         0.300         0.195         0.286         0.216         0.303         0.207         0.306         0.232           yg         0.165         0.261         0.167         0.264         0.157         0.251         0.173         0.266         0.170         0.275         0.194           6         0.378         0.281         0.395         0.283         0.356         0.245         0.399         0.257         0.373         0.280         0.438           026         0.404         0.281         0.410         0.290         0.385         0.245         0.394         0.268         0.390         0.288         0.446           06         0.404         0.280         0.414         0.295         0.398         0.262         0.413         0.278         0.407         0.299         0.461           00         0.446         0.304         0.445         0.311         0.439         0.284         0.449         0.299         0.438         0.310         0.494	20         0.204         0.295         0.207         0.300         0.195         0.286         0.216         0.303         0.207         0.306         0.232         0.319           yg         0.165         0.261         0.167         0.264         0.157         0.251         0.173         0.266         0.170         0.275         0.194         0.287           6         0.378         0.268         0.395         0.285         0.245         0.369         0.257         0.373         0.280         0.438         0.291           22         0.396         0.281         0.410         0.290         0.385         0.251         0.394         0.268         0.390         0.288         0.446         0.299         0.461         0.308           06         0.404         0.280         0.414         0.295         0.398         0.262         0.413         0.278         0.478         0.299         0.461         0.300           01         0.446         0.304         0.445         0.311         0.439         0.284         0.449         0.299         0.438         0.310         0.494         0.318	20         0.204         0.295         0.207         0.300         0.195         0.286         0.216         0.303         0.207         0.306         0.232         0.319         0.192           2g         0.165         0.261         0.167         0.264         0.157         0.251         0.173         0.266         0.170         0.275         0.194         0.287         0.161           6         0.378         0.268         0.395         0.285         0.245         0.369         0.257         0.373         0.280         0.438         0.291         0.354           02         0.396         0.281         0.410         0.290         0.385         0.251         0.394         0.268         0.390         0.288         0.446         0.290         0.385         0.251         0.394         0.268         0.390         0.288         0.446         0.290         0.364           06         0.404         0.280         0.414         0.295         0.398         0.262         0.413         0.278         0.407         0.299         0.461         0.300         0.382           09         0.446         0.304         0.445         0.311         0.439         0.244         0.449	20         0.204         0.295         0.207         0.300         0.195         0.286         0.216         0.303         0.207         0.306         0.232         0.319         0.192         0.285           g         0.165         0.261         0.167         0.264         0.157         0.251         0.173         0.266         0.170         0.275         0.194         0.287         0.161         0.256           6         0.378         0.268         0.395         0.235         0.355         0.245         0.369         0.257         0.373         0.280         0.438         0.291         0.351         0.257           02         0.396         0.281         0.410         0.290         0.385         0.251         0.394         0.268         0.390         0.288         0.446         0.293         0.364         0.256           16         0.404         0.280         0.414         0.295         0.398         0.262         0.413         0.279         0.461         0.300         0.382         0.273           10         0.446         0.304         0.445         0.311         0.439         0.284         0.449         0.299         0.438         0.310         0.430	20         0.204         0.295         0.207         0.300         0.195         0.268         0.216         0.303         0.207         0.306         0.232         0.319         \undersigned{0.192}         0.285         0.233           gg         0.165         0.261         0.167         0.264         \undersigned{0.1577}         \undersigned{0.257}         0.170         0.275         0.194         0.287         0.161         0.256         0.177           6         0.378         0.288         0.395         0.238         0.355         0.245         0.369         0.287         0.338         0.291         0.351         0.257         0.410           22         0.396         0.281         0.410         0.290         0.385         0.245         0.394         0.268         0.390         0.288         0.440         0.290         0.384         0.291         0.351         0.257         0.410           22         0.396         0.281         0.410         0.290         0.388         0.268         0.390         0.288         0.446         0.293         0.364         0.265         0.423           60         0.404         0.280         0.414         0.295         0.398         0.262	$\begin{array}{c ccccccccccccccccccccccccccccccccccc$	$\begin{array}{c ccccccccccccccccccccccccccccccccccc$	$\begin{array}{c ccccccccccccccccccccccccccccccccccc$	0

Table 12: Performance comparison between MLLM4TS and OFA (Zhou et al., 2023) on few-shot forecasting. 10% of the training data is used to train the model. We mark the better performance in **bold**.

Method	Horizon	MLL	M4TS	0	FA
	Metric	MSE	MAE	MSE	MAE
	96	0.164	0.219	0.161	0.212
	192	0.202	0.247	0.207	0.253
Weather	336	0.258	0.295	0.264	0.298
	720	0.322	0.338	0.321	0.335
	Avg	0.236	0.274	0.238	0.275
	96	0.494	0.489	0.464	0.472
	192	0.522	0.509	0.526	0.507
ETTh1	336	0.534	0.511	0.747	0.601
	720	0.761	0.633	0.769	0.632
	Avg	0.578	0.535	0.626	0.553

Table 13: Performance overview on zero-shot forecasting. For MLLM4TS and OFA, the model is trained on ETTh2 dataset and then tested on ETTh1 dataset. For time series foundation models pretrained from time series corpus, the models are directly applied on ETTh1 dataset. The best performance is highlighted in **bold**, and the second-best is <u>underlined</u>.

Dataset	Horizon	MLLM4TS		OFA (2023)		Chronos (2024)		Moirai (2024)		MOMENT (2024)		LLMTime (2023)	
		MSE	MAE	MSE	MAE	MSE	MAE	MSE	MAE	MSE	MAE	MSE	MAE
	96	0.503	0.488	0.459	0.458	0.441	0.390	0.38	0.388	0.688	0.557	1.130	0.777
	192	0.454	0.459	0.496	0.481	0.502	0.524	0.434	0.415	0.688	0.560	1.242	0.820
$ETTh2 \rightarrow ETTh1$	336	0.518	0.496	0.537	0.517	0.576	0.467	0.485	0.445	0.675	0.563	1.328	0.864
	720	0.521	0.517	0.604	0.556	0.835	0.583	0.61	0.510	0.683	0.585	4.145	1.461
	Avg	0.499	0.490	0.524	0.503	0.588	<u>0.466</u>	0.480	0.430	0.683	0.560	1.961	0.981

The consistent performance improvements over the time-series-only counterpart underscore the effectiveness of incorporating a vision modality into time-series analysis. Ablation results across different model variants further validate the robustness of the proposed framework. An alternative to LLM-based direct forecasting is the autoregressive approach, where future values are generated sequentially based on previously predicted outputs, as suggested by recent work (Liu et al., 2024e). As shown in Table 16 ('AutoReg'), this method performs well for short prediction horizons but suffers from error accumulation as the forecasting window lengthens, leading to degraded performance. Moreover, increasing the language model size from GPT-2 (Radford et al., 2019) (124M parameters) to larger models such as Qwen3 (Yang et al., 2024) (1.7B parameters) does not yield further gains in multimodal time-series tasks. These findings suggest that smaller models provide sufficient language modeling capacity, while larger models may be more prone to overfitting noise in time-series data, potentially hindering generalization.

Table 14: Ablation study on time-series classification task. 'LLM2Attn' replaces the language model with one single attention layer. 'Layout' replaces horizontal layout with grid layout. 'VisualEnc' replaces CLIP with ResNet. 'Fusion' replaces early fusion with late fusion.

Dataset	Т	S-Only					
	OFA	LLM2Attn	MLLM4TS	Layout	VisualEnc	Fusion	LLM2Attn
EC	33.1	33.1	38.8	41.1	34.1	35.0	33.8
FD	69.2	66.1	68.5	58.7	68.6	58.0	60.2
HW	30.9	32.9	40.0	43.1	34.2	33.9	32.6
HB	78.0	75.6	80.0	80.5	78.1	80.0	77.6
JV	82.4	93.8	99.7	99.2	98.7	99.2	98.4
PSF	87.9	89.0	94.2	89.0	85.6	86.7	83.8
SRSCP1	93.5	93.2	93.2	91.1	90.1	89.8	91.8
SRSCP2	60.1	57.2	60.6	62.2	57.2	64.4	56.7
SAD	99.3	73.8	99.6	99.1	87.7	96.3	87.3
UWGL	86.9	87.2	92.8	87.9	91.9	91.3	91.6
Average	72.2	70.2	76.7	75.2	72.6	73.5	71.4

Table 15: Ablation study on time-series anomaly detection task. 'LLM2Attn' replaces the language model with one single attention layer. 'Layout' replaces horizontal layout with grid layout. 'Visua-lEnc' replaces CLIP with ResNet. 'Fusion' replaces early fusion with late fusion.

Domain	T	S-Only	Plot-TS						
	OFA	LLM2Attn	MLLM4TS	Layout	VisualEnc	Fusion	LLM2Attn		
Environment	0.909	1.000	1.000	1.000	1.000	1.000	0.886		
Facility	0.647	0.599	0.679	0.678	0.692	0.679	0.692		
Finance	0.156	0.154	0.143	0.145	0.145	0.149	0.222		
HumanActivity	0.110	0.102	0.122	0.120	0.122	0.120	0.092		
Medical	0.083	0.085	0.131	0.134	0.139	0.133	0.163		
Sensor	0.125	0.117	0.194	0.180	0.181	0.179	0.164		
Average	0.296	0.286	0.349	0.344	0.348	0.343	0.340		

# C SHOW CASE

We provide example time series plots in Section C.1 and an illustration of the attention map for multi-modal tokens in language models in Section C.2.

# C.1 EXAMPLE PLOTS

We provide an illustration of horizontal and grid layout in Figure 9, and example plots of datasets used in this work in Figure 10.

Table 16: Ablation study on time-series forecasting task. 'AutoReg' trains the model and generates forecasting results in an autoregressive manner as described in AutoTimes (Liu et al., 2024e). 'VisualEnc' replaces CLIP with ResNet. 'Fusion' replaces early fusion with late fusion. 'LLM2Attn' replaces the language model with one single attention layer.

Dataset	ETTh1								Weather							
Type	MLL	M4TS	Auto	oReg	Visua	alEnc	LLM	2Attn	MLL	M4TS	Auto	Reg	Visua	alEnc	LLM	2Attn
Metric	MSE	MAE	MSE	MAE	MSE	MAE	MSE	MAE	MSE	MAE	MSE	MAE	MSE	MAE	MSE	MAE
Pred-96	0.366	0.4	0.361	0.394	0.397	0.423	0.479	0.483	0.149	0.198	0.149	0.201	0.165	0.217	0.187	0.243
Pred-192	0.404	0.42	0.397	0.417	0.436	0.593	0.495	0.509	0.193	0.245	0.202	0.248	0.227	0.271	0.225	0.273
Pred-336	0.425	0.434	0.42	0.433	0.475	0.477	0.506	0.522	0.243	0.282	0.263	0.291	0.269	0.307	0.267	0.303
Pred-720	0.436	0.467	0.446	0.46	0.515	0.514	0.540	0.561	0.315	0.337	0.336	0.343	0.331	0.352	$\underline{0.328}$	0.347

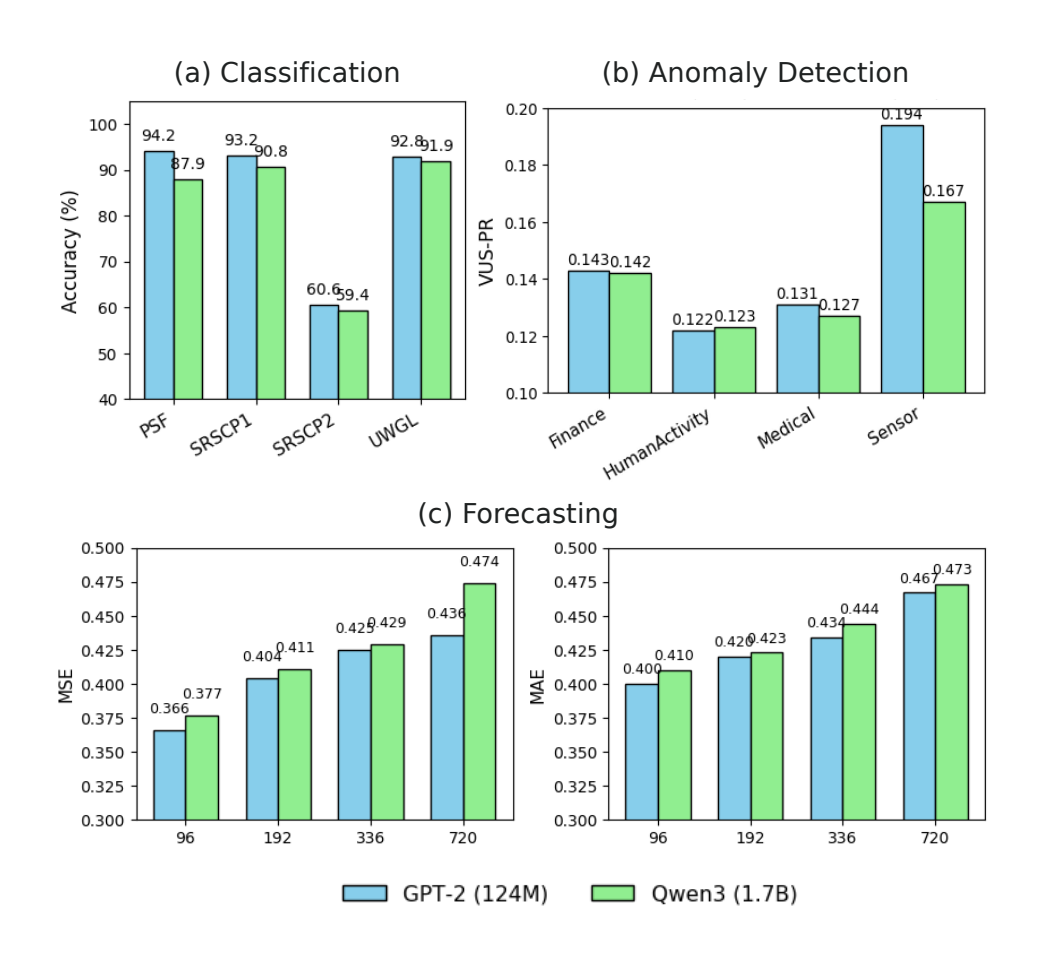


Figure 8: Comparison of task performance using different language model backbones: GPT-2 (Radford et al., 2019) (124M parameters) and Qwen3 (Yang et al., 2024) (1.7B parameters). Panels (a) classification and (b) anomaly detection show metrics for which higher values indicate better performance, while panel (c) forecasting presents forecasting errors, where lower values denote better results.

Table 17: Impact of Dimensionality Reduction. MLLM4TS (Dim.) refers to reducing the plotted channels to 50 by removing highly correlated time-series channels, whereas MLLM4TS (Orig.) denotes visualization using all original channels.

Method	Horizon	MLLM	4TS (Dim.)	MLLM4TS (Orig.)			
	Metric	MSE	MAE	MSE	MAE		
	96	0.134	0.232	0.141	0.244		
	192	0.153	0.251	0.157	0.253		
ECL	336	0.169	0.267	0.168	0.263		
	720	0.204	0.295	0.201	0.293		
	Avg	0.165	0.261	0.166	0.263		
	96	0.378	0.268	0.386	0.281		
	192	0.396	0.281	0.399	0.289		
Traffic	336	0.404	0.28	0.420	0.304		
	720	0.446	0.304	0.449	0.308		
	Avg	0.406	0.283	0.414	0.295		

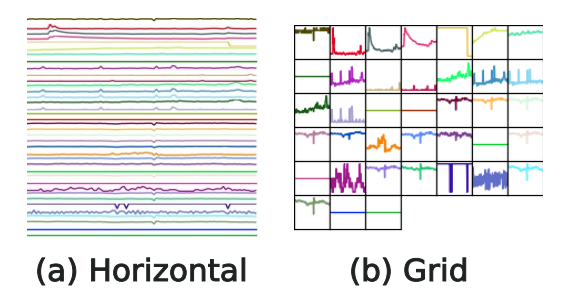


Figure 9: Example plots of (a) horizontal and (b) grid layout.

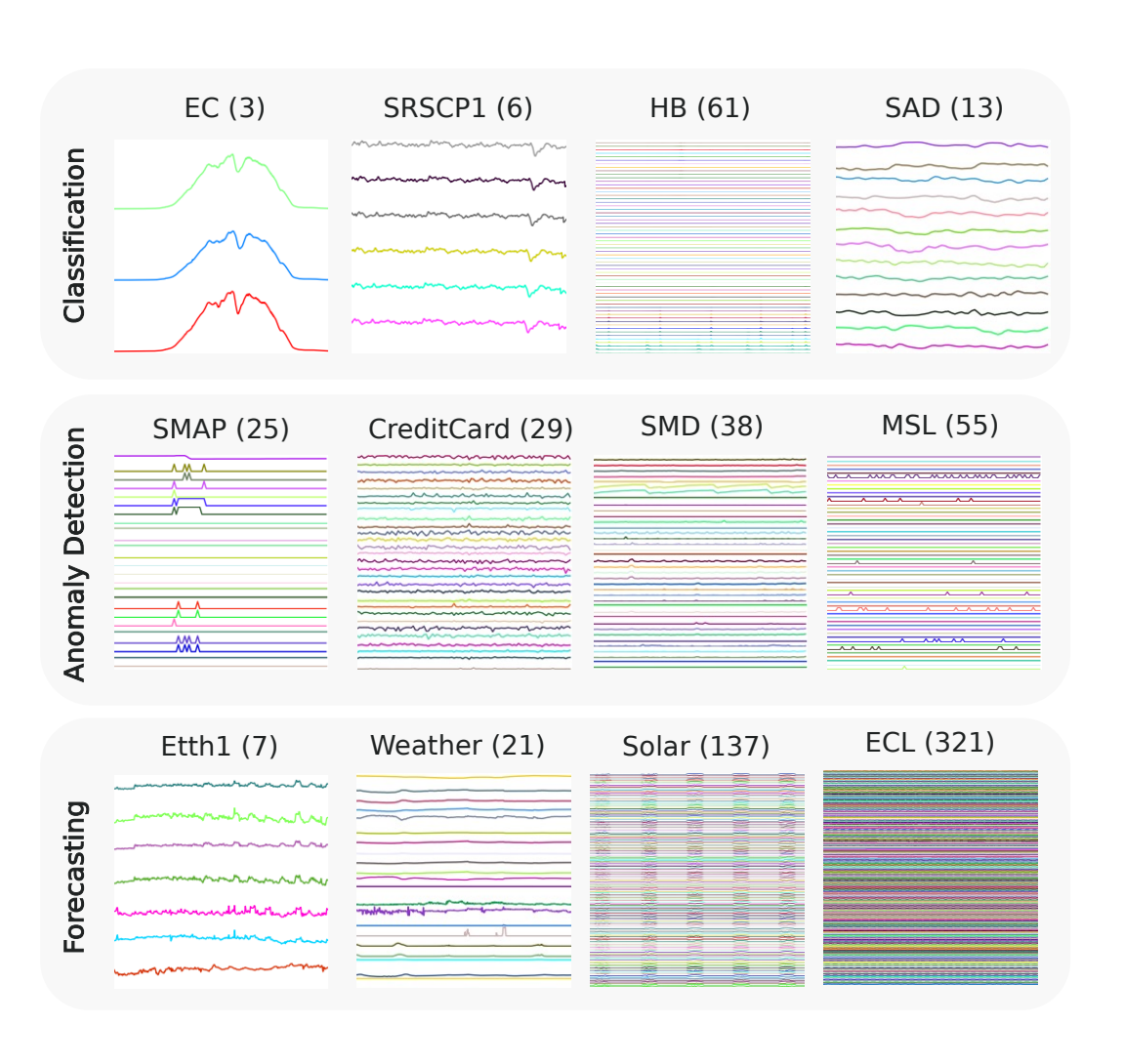


Figure 10: Example plots of an instance from datasets used in this work (dataset name and channel count in parentheses).

# C.2 ATTENTION MAPS

To better understand how the language model processes multimodal input, we visualize the attention maps of the language model backbone. The input consists of a concatenation of time-series tokens  $(TS_1, \ldots, TS_N)$  and visual tokens  $(V_1, \ldots, V_M)$ . In the early transformer layers, attention is primarily concentrated on the time-series tokens, with limited attention directed toward the visual tokens. As the depth of the model increases, attention becomes more evenly distributed across both modalities, indicating that cross-modal interactions become more prominent in the deeper layers of the language model.

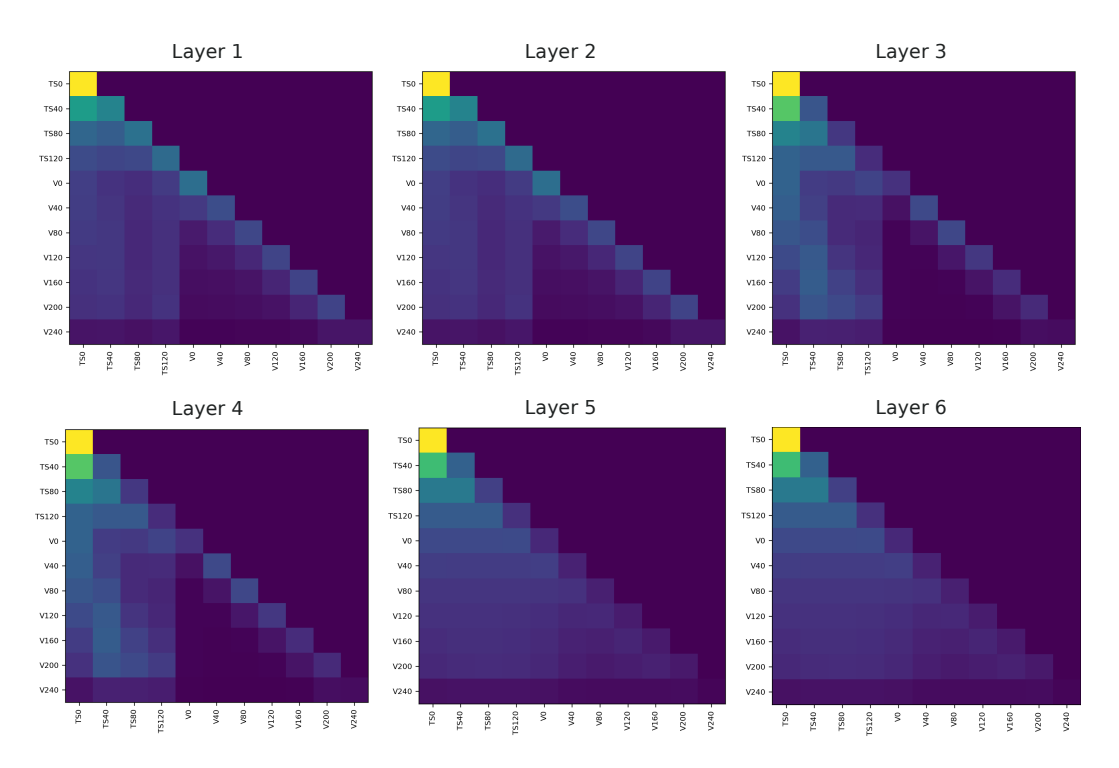


Figure 11: Layer-wise self-attention maps of the language model in MLLM4TS (Late) for the classification task. Each heatmap displays the average attention weights over the entire test set. The input tokens are concatenated time-series tokens  $(TS_1, \ldots, TS_N)$  and visual tokens  $(V_1, \ldots, V_M)$ .

# C.3 IMPACT OF CHANNEL COLOR CODING

We further investigate the impact of channel-specific color coding in time series plots. As illustrated in Figure 12, we compare three configurations: (1) MLLM4TS with color-coded channels, (2) MLLM4TS without color coding, and (3) a time-series-only baseline. The version of MLLM4TS without color coding achieves intermediate performance between the other two settings. This suggests that while the inclusion of visual representations alone provides benefits, applying channel-wise color coding enhances the model's ability to capture cross-channel dependencies, demonstrating the effectiveness of the proposed design.

# D BROADER IMPACT

**Impact on Real-world Applications.** MLLM4TS offers a unified and effective solution for a wide range of time series analysis tasks, including but not limited to classification, anomaly detection, and forecasting. These capabilities support practical applications in domains such as electrocardiogram monitoring, human activity recognition, financial modeling, facility management, environmental sensing, and industrial process control. Its strong performance in few-shot and zero-shot scenarios,

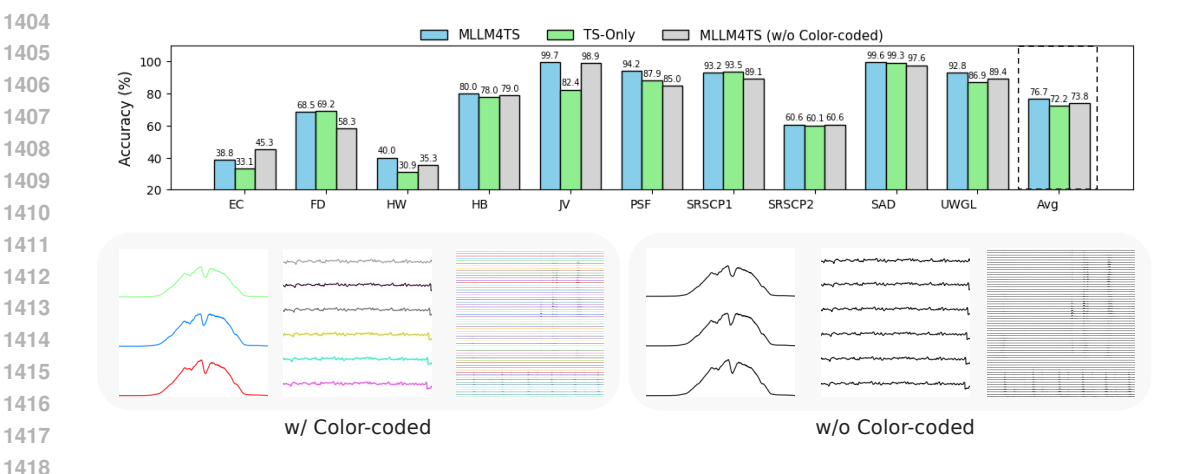


Figure 12: Impact of channel color coding on time series classification performance.

together with its robustness to hyperparameter variation (such as patch size), highlights its reliability in data-sparse environments. These characteristics make MLLM4TS a strong candidate for deployment in decision support systems across healthcare, manufacturing, finance, and climate-related services.

**Impact on Future Research.** This work is among the first to incorporate line plots, an intuitive and widely used method for visualizing time series, into the context of multi-modal time series analysis. While the proposed framework focuses on line plot representations, its architecture can be extended to incorporate aligned image and video data. Furthermore, our investigation into the roles of visual representations and language model backbones provides valuable insights for the development of explainable and agentic time series analysis, paving the way for safer and more transparent deployment in high-stakes domains.

# E LIMITATION AND FUTURE WORK

One limitation of MLLM4TS is the additional computational overhead introduced by the vision branch, which increases runtime during the processing of visual embeddings. Future research may explore the design of more lightweight visual frontends for rendering visual representations, with the goal of improving runtime efficiency. Another promising direction is extending MLLM4TS to handle irregularly sampled time series. Given the demonstrated benefits of visual representations, converting such data into image form may offer a more natural solution, opening new avenues for multimodal time-series analysis in this context.